NUMERICAL AND EXPERIMENTAL STUDY ON DYNAMICS OF UNSTEADY PIPE FLOW INVOLVING BACKFLOW PREVENTION ASSEMBLIES

by

HYOUNG-JIN KIM

A Dissertation Presented to the

FACULTY OF THE USC GRADUATE SCHOOL

UNIVERSITY OF SOUTHERN CALIFORNIA

In Partial Fulfillment of the

Requirements for the Degree

DOCTOR OF PHILOSOPHY

(CIVIL ENGINEERING)

December 2012

Acknowledgements

First, I would like to thank my advisor, Dr. Jiin-Jen Lee, for his continuous supports and efforts during my academic years at University of Southern California. Whenever I doubt myself, he was there encouraging me not to loose goals academically and personally. I have learned from him how to look a problem in a big picture, how to solve it efficiently, and how to express an idea in an effective manner.

I also would like thank the staff members (at the Foundation of cross connection control and hydraulic research) for giving the opportunity for testing utilities and providing the valuable information of testing equipments and experimental data.

A special thank to my dad for his unconditional support and trust with his generous mind. Without him, nothing would have be possible for my life.

Last, but not least, I would like to thank my beloved family, Jungwan, Noah, and Sarah who have endured suffering with patience and faith over last years of study.

Contents

List of Tables

List of Figures

Abstract

When control valves at the end of pipeline close simultaneously, two pressure waves are generated at each end and the waves propagate toward to the other end. The pressure waves continue to move back and forth along pipelines until they are damped out to next steady states. This study provides information on the experimental data and the numerical simulation of a rapid hydraulic transient event called water hammer. The energy loss term due to friction in the present model consists of quasi-steady contribution and unsteady contribution. For the present model, an equivalent friction coefficient is used to replace the quasi-steady friction coefficient, inclusive unsteady friction loss and minor energy loss factors. The unsteady component has been related to the combination of the instant flow acceleration and instant flow convective acceleration. The numerical results of the present model are compared with the experimental records. The computer results by the present model which is based on the unsteady friction 1D model was successful to follow general trends of water hammer phenomena, corresponding with sudden changes in flow. This study later extends to the dynamic characteristics of backflow prevention assemblies under a rapid transient condition. When numerous hydraulic devices are

installed on water distribution systems, the dynamic characteristics of such hydraulic devices have a significant influence on the intensity of the associated water hammer waves. A backflow prevention assembly plays important roles as not only a safety hydraulic device but also an energy dissipater. A numerical program for rapid transient pipe flow interconnected with a backflow prevention assembly has been developed using the present coupling model and numerically solved by the method of characteristics.

Chapter 1

Introduction

1.1 Background

Drinking water distribution systems are large networks of piping systems designed to transport drinkable water from sources to consumers. A water distribution system consists of storages (reservoirs or water tanks), pumps, networks of pipes, control valves and other hydraulic appurtenances. The primary function of drinking water distribution systems today is to deliver water of good quality efficiently and safely to the end of water users. Early water distribution systems were run solely by gravity at a relatively low pressure. The supply of water was restricted low because of the limited water sources reliable and the limited technologies available. For these reasons steady conditions were prevalent throughout the systems. As a continuous demand for water has increased due to fast growing population, there has been a growing need of improved water delivering systems which are operated under a high pressure and a high flow rate. Today water distribution systems, therefore, have been enhanced by equipping with a series of pumps, a intricate network of pipelines, and numerous hydraulic devices. Unavoidably, transient conditions are of great possibility everywhere in modern water distribution systems. A wide variation of water usages often causes extreme pressure fluctuations through the system. For example, sudden stoppage of pumps (pump failure), immature operations of valves and the influence of accidental events such as power outages and burst pipes, all of these create transient flow conditions. Many literature and the public press have reported a large number of incidents of hydraulic transients in the water distribution systems over the last century. Many safety devices have been developed and installed to prevent water accidents and/or to minimize the further system damages in case of the accidents.

Maintaining water distribution systems under normal operating condition as designed is crucial to ensuring safe drinking water and its supply systems against contamination and damage respectively. Thus, the importance of hydraulic transient analysis in water distribution systems has been arisen and further research of transient pipe flow should be taken into account. Today, modeling of the systems is a fundamental part in providing basis for planning and designing to engineers and implementing the right decisions to operators.

Sudden momentum changes in fluid in motion creates excessive pressure changes (positive and negative pressure surges) inducing backflow into attached water piping systems. This rapid transient event is a phenomenon called water hammer. Traditionally friction losses in the simulation of water hammer has been modeled using steady friction approximation such as Darcy-Weisbach equation, which is known as quasi-steady approximation. It is widely known that this assumption gives a satisfactory result only for slow transients where the wall shear stress has a quasi-steady behaviour. This quasi-steady friction approximation uses the friction coefficient (named Darcy-Weisbach friction coefficient) depending on the state of the system at the previous time step. Even though the friction coefficient used in this model is estimated by means of an approximated formula of the Moody diagram for each time step, it would be not valid for the simulation of transients because the value of the coefficient is estimated on the basis of initial steady flow Q_0. The experimental validation of this study shows that the quasi-steady approximation shows a poor agreement between the experimental data and computer calculation, in magnitude and phase of pressure waves particularly for long-time-period records of rapid transient events. Good estimation of friction losses under transient conditions is one of the key issues encountered in the development of understanding and modeling of rapid transient pipe flows in the systems. Thus, further investigation of unsteady friction effect in rapid transients of a simple reservoir-pipe-valve system are presented in this study. Two one-dimensional unsteady friction models, the Zielke [29] and the Brunone et al [1],[2] models, are reviewed in detail in the later chapter. Finally, the Brunone unsteady friction model is incorporated with the pipe equations(water hammer equations) and the valve equations for the analytic solution of the equations for unsteady pipe flow interacted with backflow prevention assemblies. The derivation of this model is presented in detail in chapter 3.

In order to prevent backflow from occurring in distribution systems, backflow preventers are required and are installed between the delivery point of water mains and local storage or use. The basic method of preventing backflow is an air gap. This method eliminates a direct cross-connection between a contaminated water source and a potable source by providing an adequate space between them. However, an air gap loses the pressure in the pipe system (drop to atmospheric pressure). Thus different backflow preventers are used to protect the water distribution system. Backflow prevention assemblies are mechanical devices that provide a physical barrier to backflow. In general, a backflow prevention assembly consists of a combinations of check valves, relief valves, air inlet valves and/or shutoff valves. The types of backflow prevention assemblies would be classified, according to the types of internal valves used. There are four types commonly used.

- Reduced Pressure Principle Assembly (RP)
- Double Check Valve Assembly (DC)
- Pressure Vacuum Breaker (PVB)
- Atmospheric Vacuum Breaker (AVB)

The most important considerations in selecting a backflow prevention assembly, are the head loss and non-slamming characteristics. It should have an acceptable head loss coefficient for forward flow under normal flow condition, and not create excessive transient pressures under the reverse flow condition upon a sudden closing.

The dynamic characteristics of backflow prevention assemblies depends mainly on the internal check valves used. The valve position under the transient flow condition is determined by the flow and valve dynamics. The dynamic behavior of backflow prevention assemblies is studied by using both experimental and theoretical approaches. Accurate modeling of the dynamics of a backflow prevention assembly requires experimental data to quantify coefficients for the hydraulic torque term in the moment-of-momentum equation. Based on the understanding of the dynamic interaction between the flow and an internal check, a final numerical model is developed coupling those equations of motion of checks into the unsteady model.

For the present study, a numerical solution for unsteady pipe flow for the reservoir-pipe-valve system is obtained by using the method of characteristics. A pair of partial differential equations for unsteady pipe flow may be transformed into four ordinary differential equations by the method of characteristics. Those ordinary equations may be integrated to achieve numerical solutions by finite differential method.

1.2 Literature Review

Two differential equations for unsteady pipe flows are derived in this section based on the classic water hammer theory. The governing equations are namely the conservation of mass and the conservation of momentum. A set of water hammer equations can be modified by making several assumptions on the flow condition. Then, several unsteady friction models are reviewed. The Quasi-steady model has been used to quantify the system's friction coefficient, F_T for transient flow. And unsteady friction models by Zielke [29], Vardy [25], [26], and Brunone et al. [1], [2] are introduced and the Brunone model has been selected for later use in this study.

1.2.1 Fundamental Partial Differential Equations

The momentum and continuity equations are a set of non-linear, hyperbolic, partial differential equations that govern unsteady flow in a closed conduit. Among the early researchers of water hammer problems, Joukowsky (1898) [8] produced the well-known equation that relates pressure changes, ΔP, to velocity changes, ΔV, according to Eqn 1.1. This equation was developed based on the rigid column theory in which the compressibility of water and elasticity of pipe wall are ignored.

$$\Delta P = \pm \rho a \Delta V \; or \; \Delta H = \pm \frac{a \Delta V}{g} \tag{1.1}$$

where ρ is the fluid density, H is the piezometric head, and a is the speed of sound. Kortewegs (1878) formula defines the wave speed a for fluid in cylindrical pipes as

$$a = \sqrt{K'/\rho} \; and \; K' = \sqrt{\frac{K}{(1 + (DK)/(eE))}} \tag{1.2}$$

where D is the diameter of the pipe, e is the wall thickness, E is the modulus of elasticity for the wall, and K is the bulk modulus of elasticity of fluid. Further investigation to the governing equations of water hammer has continued by many researchers (Jaeger [6], [7], Wood [27], Rich [16],[17], Parmakian [12], Streeter and Lai [18], and Streeter and Wylie [19]), resulting in the following the classical water hammer equations for one-dimensional unsteady pipe flows.

1.2.2 Classic Water Hammer Theory

Fully developed by 1960s the classical water hammer equations may be able to describe general physics necessary to model wave generation, propagation, and energy damping in water distribution systems. However, it is widely known today that the model based on quasi-steady friction losses hypothesis shows the basic reasons for differences between experimental and computational results obtained according to the classical water hammer theory. Numerous researchers has developed miscellaneous unsteady friction models that consider extra parameters affecting on the unsteady friction losses. The classical Water hammer equations are presented in this chapter and several unsteady friction models are derived, being modified from the classical water hammer equations by using different approaches. Here, two governing equations based on the classic water hammer theory may be applied for calculation of the liquid unsteady pipe flow. The assumptions made in the development of equations are

- The flow velocity and pressure at a cross-section are averaged and uniform (one-dimensional).
- The fluid is slightly compressible.
- The pipe is full and remains full during the transient.
- The pipe wall is linearly elastic and slightly deformable.
- Free gas content of the liquid is small such that the wave speed can be regarded as a constant.

These assumptions have been well adopted for many numerical analysis tools for unsteady pipe flows. The fundamental governing equations under the assumptions are described by the continuity and motion equations [28], [4]. The conservation of mass for one-dimensional unsteady pipe flow is represented by

$$\frac{\partial P}{\partial t} + V\frac{\partial P}{\partial x} - \rho g V sin\theta + \rho a^2 \frac{\partial V}{\partial x} = 0 \tag{1.3}$$

where

P = pressure

V = average velocity

a = wave speed

ρ = fluid density

g = gravitational acceleration

θ = angle at which pipeline is inclined with the horizontal

t = time

x = distance

and wave speed is calculated using Eqn 1.2. The wave speed in a closed conduit can be evaluated by investigating the fluid properties and conduit's elasticity as given by $\Delta A/\Delta pA$ in Eqn 1.2 depending on

1. Fluid Properties

    - Modulus of elasticity
    - Density
    - Amount of air, and so forth

2. Pipe properties

    - Modulus of elasticity

- Diameter
- Thickness

For very thick-walled pipe $\Delta A/\Delta p$ is very small, and $a \approx \sqrt{k/\rho}$ is the acoustic speed of a small disturbance in an infinite fluid. For very flexible pipe walls, the second term in the denominator is relatively large and the wave speed becomes Eqn 1.4. For the computer model presented in this study, a special formula for wave speed under the pipe wall condition is used and it is expressed in Eqn 1.4 for calculation.

$$a = \sqrt{\frac{K_w/\rho_w}{1 + (1-p^2) * (K_w/E_p) * (D/e)}} \tag{1.4}$$

where

K_w = Bulk modulus for water

ρ_w = Density of water

p = Poisson's ratio for pipe material

E_p = Young's modulus for pipe material

D =Pipe Diameter(m)

e = Pipe thickness(m)

For water under ordinary condition the wave speed can be calculated by $\sqrt{K/\rho} = 1440 m/s$. The speed of pressure waves is assumed to be maintained a constant value for the present models. However, However, the measured data shows a significant reduction in the wave speed in transitional zone, causing an observable phase shift.

The piezometric head may replace pressure with the relation of

$$\partial P/\partial t = \rho g(\partial H/\partial t) \tag{1.5}$$

For most engineering applications, the convective term $V\,(\partial H/\partial x)$ and $V sin\theta$ are negligible compared to the other terms and may be neglected. Eqn 1.3 becomes

$$\frac{\partial H}{\partial t} + \frac{a^2}{g}\frac{\partial V}{\partial x} = 0 \tag{1.6}$$

This is a simplified hydraulic-grade-line form of the continuity equation for unsteady flow, Eqn 1.6.

The equation of motion for fluid flowing through a pipe is presented in Eqn 1.7. An average cross-sectional pressure equal to the centerline pressure $p(x,t)$ and an average cross-sectional velocity $V(x,t)$ are assumed in the one-dimensional equation derivation.

$$\frac{1}{\rho}\frac{\partial P}{\partial x} + V\frac{\partial V}{\partial x} + \frac{\partial V}{\partial t} + g\sin\theta + F = 0 \tag{1.7}$$

where

θ = angle at which pipeline is inclined with the horizontal

F = head losses per unit length due to friction

When the convective term $V(\partial V/\partial x)$ is assumed negligible, the pipeline is horizontal ($\sin\theta = 0$), and pressure is replaced by the piezometric head in the same manner as in the equation of continuity, the equation can be further reduced to

$$g\frac{\partial H}{\partial x} + \frac{\partial V}{\partial t} + gF = 0 \tag{1.8}$$

which is the simplified hydraulic-grade-line form of the equation of motion. F in Eqn 1.8 is considered as a sum of the head loss due to steady and unsteady friction, respectively.

$$F = F_{steady} + F_{unsteady} \tag{1.9}$$

The steady component of the friction may be based on the Darcy-Weisbach friction relationship and is defined as

$$F_{steady} = \frac{f}{D} \frac{V\,|V|}{2g} \tag{1.10}$$

in which

f = Darcy-Weisbach friction factor

D = Pipe diameter.

A common friction modeling according to the quasi-state flow hypothesis assumes that $F_{unsteady}$ equals zero. In addition, a miscellaneous unsteady friction models considering extra unsteady friction losses have been developed for many years in a large number of literature. Two distinct modeling approaches compress several unsteady friction models into two main groups of research.

1.2.3 Friction Models Used In Calculation

After created in the pipe systems, pressure waves propagate along the pipeline and dissipate after a short period of time, consequently reaching to another steady state. It comes from the hydraulic resistance caused by both the internal friction of the fluid and the friction at pipe walls. The quasi-steady friction model and two distinct unsteady friction models are presented in this chapter.

The quasi-steady method assumes that unsteady friction factor has no contribution to energy loss. Thus, the quasi-steady model uses F_{steady} only. This quasi-steady friction model is computationally economical and effective. However, its numerical results always underestimate the energy losses due to friction during hydraulic transients.

$$F = F_{steady} = \frac{f}{D}\frac{V\left|V\right|}{2g} \tag{1.11}$$

In the first group of research the unsteady friction is calculated on the basis of the past flow acceleration (Zielke [29], Trikha [22], Vardy and Brown [23], [24], [25], [26]). Zielke [29] developed an analytical model in which the unsteady head loss term, $F_{unsteady}$, is a function of flow acceleration and weighted past velocity changes. The unsteady head loss per unit length is expressed by

$$F_{unsteady}(t) = \frac{16\nu}{gD^2}\int_0^t \frac{\partial V}{\partial t}(u) * W(t-u)du \tag{1.12}$$

where ν= kinematic viscosity; W= weighting function; and $*$= convolution operator. The convolution integral is approximated using the rectangular rule and the acceleration term is approximated using a centered finite difference as

$$F_{unsteady}(t)_{app} = \frac{16\nu}{gD^2}\sum_{j=1,3,5,\cdots}^{M}\left[V(t-j\Delta t+\Delta t) - V(t-j\Delta t-\Delta t)\right]W(j\Delta t) \tag{1.13}$$

where $M = t/\Delta t - 1$. Zielke [29] determined a weighting function applicable to laminar flows and Trikha [22] developed a simplified model based on the Zielke's work, allowing saving a lot of computing power and time. Whereas the previous models were only applicable to laminar flows, Vardy and Brown improved the weighting function applicable for smooth-pipe turbulent flows [23], [24] and rough-pipe turbulent flows [26]. However, Vardy and Brown showed the results of computation only in short duration of time. The trend of energy decay in transient flow cannot be fully observed in such a short time duration. Also, this model is valid only for low Re number.

In the second group the unsteady friction is related to the instantaneous acceleration (Daily et al. [9], Brunone et al. [1], [2]). The dependence of unsteady friction on acceleration was initiated by Daily et al. [9]. In their model a result of experimental work defines the unsteady friction term as

$$F = \frac{f}{D}\frac{V^2}{2g} + \frac{k_1}{g}\frac{dV}{dt} \tag{1.14}$$

where the dimensionless coefficient k_1 is equal to 0.01-0.015 for accelerating flow and 0.62 for decelerating flow. Carstens and Roller [3] suggested the value of k_1 is a function of Reynolds number Re.

Brunone et al. [2] introduced an additional convective acceleration term to keep unsteady friction when $V\partial V/\partial t > 0$ and to cancel it when $V\partial V/\partial t < 0$. The non-linear term, $\partial V/\partial x$, that was ignored due to its small value in the process of derivation of classical water hammer equations, is now multiplied by the wave speed, a, and added to the instant acceleration term, $\partial V/\partial t$. The combination of two acceleration terms is then multiplied by a constant coefficient, k_2 for the unsteady friction model.

$$F = \frac{f}{D}\frac{V^2}{2g} + \frac{k_2}{g}\left(\frac{\partial V}{\partial t} - a\frac{\partial V}{\partial x}\right) \tag{1.15}$$

in which the coefficient k_2 is originally evaluated by the experiment. The role of the coefficient, k_2 is very important for this model. This coefficient may be assumed constant or depending on the initial Re value. Since unsteady friction models based on instantaneous values of the flow are relatively simple and computationally effective, the Brunone's model is selected and modified for later use in this study.

1.2.4 Dynamics Involving Backflow Prevention Assemblies

A literature review on dynamics of check valves is presented for studying backflow prevention assembly's behavior during the transients in this section. In general, two lines of research have been distinguished for many years. First is the dynamic characteristics method and second is the moment-of-momentum equation method.

The dynamic characteristics method was initiated by Provoost [13], [14], [15] and widely adopted in early 1980's among researchers and manufacturers. The dynamic characteristic curve is determined experimentally. Given the flow deceleration, the maximum reverse flow velocity can be obtained from the curve. Assuming the valve is forced to close by the reverse flow, a maximum pressure peak is then calculated by using the Joukowski formula. Thorley [21], [20] presented a plot of the dynamic characteristics for various types of valves by collecting data from several sources. Koetizer et al. [5] introduced a dimensionless form of dynamic characteristics curve. From Fig 1.1, basic understandings of a non-return valve type may be obtained. An ideal backflow prevention assembly may be one which closes at the instant when the flow velocity at the assembly reaches to zero. However, limited reverse flow will still occur in the system due to the inertia and friction of the components. Some assemblies are spring-loaded or power operated for more rapid closure so that to minimize the occurrence of backflow. For a system where the flow reverses slowly, most assembles will close before any significant backflow occurs. If flow reversal occurs rapidly, a relative high reverse velocity may occur before closure causing another water hammer in the system. For a given valve, the maximum reverse velocity is a function of the rate change of backflow. Most backflow

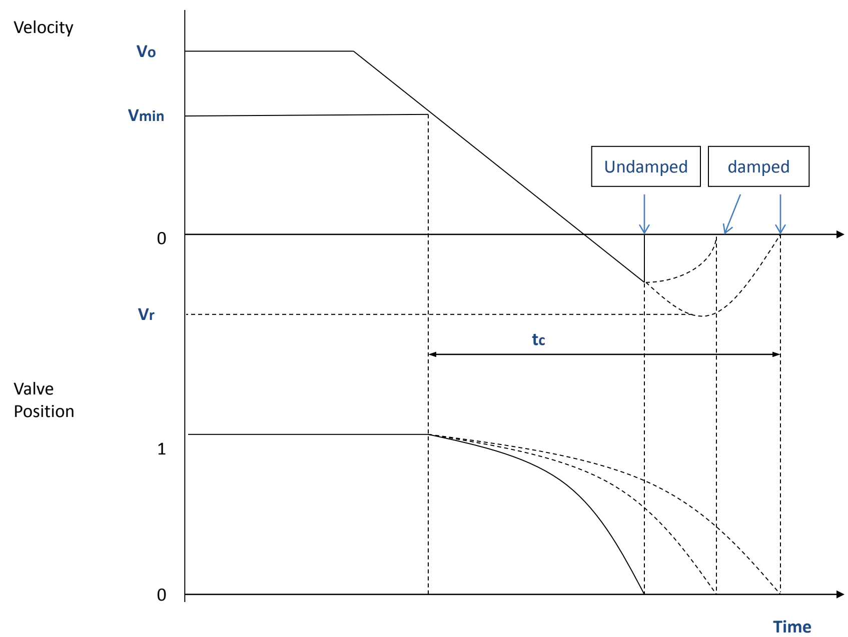

(a)V_o: initial flow Velocity (b)V_{min}:minimum velocity to keep the valve fully open

(c)V_r: maximum velocity of reverse flow (d)t_c: time of closure

Figure 1.1: Dynamic Characteristics of A General Non-return Valve

prevention assemblies are types of undamped that they close in such a way that the flow changes from the reverse V_r to zero rapidly (Fig 1.1).

All these attempts counted only for cases where flow deceleration in a pipe system is constant. Therefore, the dynamic characteristic method restricts to system-dependent problems. The dynamic behaviors of backflow prevention assemblies can be described by using the moment-of-momentum equation of a valve disk which spin-moves around a fixed hinge. In this equation, the net torque applied to a moving check disk is equated to the inertia torque. Among the net torque, a weight torque, a friction torque, and external torque can be determined theoretically in a straightforward way. The hydraulic torque, by contrast, is nearly impossible to quantify analytically or experimentally due to the complex of transient flow pattern. For the present study, the hydraulic torque is estimated by the difference of pressures calculated at two locations across the check valve, proposed by Wylie [28].

1.3 Objective and Scope of Present Study

The main objective of this study is to develop a computer model to numerically solve the problem of transient flows in a simple water distribution system such as a reservoir-pipe-valve system equipped with backflow prevention assemblies.

This study is intended to facilitate calculation of transient conditions in water distribution systems more accurately and more efficiently, considering unsteady friction effects. A coupling model is then presented to investigate the relationship between the system and the hydraulic devices. Although various boundary conditions are discussed through the study, special attention is given to the dynamic behaviors of a backflow prevention assembly with a single internal check valve. The valve equation which relates the system equations for transient flows and the equation of moment-of-momentum for the assembly is used to study the interactions between the assembly and the system.

In the present study, a set of computer algorithms for transient pipe flows and the dynamic equation of a backflow prevention assembly have been developed. Numerical simulations for transient pipe flows are performed and compared with some experimental results.

Chapter 2

Water Hammer Equations

In this chapter the one-dimensional differential equations of motion and continuity for unsteady pipe flow are introduced. Also, the modified equation of motion is presented. For the computer models, the method of characteristics, as a numerical scheme, has been used in the present study. The water hammer effect can be simulated by solving the following partial differential equations.

2.1 Differential Equations For Unsteady Flow

2.1.1 Continuity Equation

The one-dimensional conservation of mass equation(continuity) for slightly compressible fluids in cylindrical tube on any slope is rewritten as

$$\frac{\partial H}{\partial t} + \frac{a^2}{g}\frac{\partial V}{\partial x} = 0 \tag{2.1}$$

with independent variables are x= distance and t= time. Other parameters are H= piezometric head, V= flow velocity, a= wave speed, and g= gravitational acceleration. Wave speed is calculated using Eqn 1.4.

2.1.2 Momentum Equation

The unsteady friction model of Brunone et al. [1] assumes the friction term consists of two components; a quasi-steady contribution, which is the traditional assumption, and an unsteady contribution, which is related to the instantaneous acceleration $\partial V/\partial t$ and the instantaneous convective acceleration $\partial V/\partial x$.

$$F = \frac{f}{D}\frac{V\,|V|}{2g} + \frac{k_2}{g}\left(\frac{\partial V}{\partial t} - a\frac{\partial V}{\partial x}\right) \tag{2.2}$$

Incorporation of Equation (2.2) into the momentum equation, the basic equation of motion is expressed as in Equation(2.3).

$$g\frac{\partial H}{\partial x} + \frac{\partial V}{\partial t} + \frac{f}{D}\frac{V\,|V|}{2} + k_2\left(\frac{\partial V}{\partial t} - a\frac{\partial V}{\partial x}\right) = 0 \tag{2.3}$$

The parameter k_2 is evaluated by comparisons between experimental and numerical results.

2.1.3 Moment-of-Momentum Equation of a Valve Disk

Although a single check valve cannot be a secure means of preventing backflow, it is an important component of backflow prevention assemblies. A check valve is designed to allow water to pass in only one desirable direction. The check valve used in this study is of hinged swing check type with spring loading.

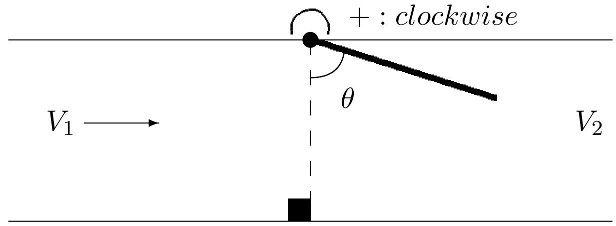

Figure 2.1: Schematic Of A Check Valve

The closing torque due to the internal spring holds the check valve closed. In order to open the check valve, the water pressure in front of the check valve or upstream must be greater than the closing torque. The dynamic behavior of a check valve can be described by the moment-of-momentum equation of the check disk. Fig.2.1 provides a schematic sketch in which θ is the disk angle, and with clockwise moments about the hinge point considered positive. The moment-of-momentum equation yields

$$T_w + T_e + T_f + T_h = I\frac{d^2\theta}{dt^2} \tag{2.4}$$

The torque due to weight of the rotating disk is given by T_w and is represented by

$$T_w = W_s r_c \sin\theta \tag{2.5}$$

in which W_s= submerged weight of the disk assembly and r_c= length from the hinge to the mass center of the disk assembly.

Any external torque applied to the disk is included in T_e. If a spring with a torsional spring stiffness of s is acting, T_e is given by

$$T_e = s\theta \tag{2.6}$$

The torque due to friction, T_f, applied at the pin joint is likely to depend on the angular velocity and it can be given by

$$T_f = k_1 + k_2 \left(\frac{d\theta}{dt} \right)^n \tag{2.7}$$

This T_f is assumed negligibly small and left out from the equation.

The torque due to the hydrodynamic pressures, T_h, is given by

$$T_h = \int_A \Delta p r dA \tag{2.8}$$

in which r is the distance to the disk area where the pressure difference across is Δp. The pressure difference is a function of the flow, the angular position, the angular speed of the disk. Since it is almost impossible to determine Δp across the disk analytically, a valve equation relating flow to pressure drop is used as

$$Q = \pm C_d A_o \sqrt{2g\Delta H} \tag{2.9}$$

in which

ΔH= the average pressure head drop across the valve

C_d= the flow coefficient

A_o= the open area through which the flow passes

and C_d is a function of the shape of flow passage and Reynolds number. If Reynolds effects are neglected, only a valve opening as a function of θ is needed.

All valves have an inherent flow characteristic that defines the relationship between valve opening and flow rate under steady conditions. Different design of the plug and

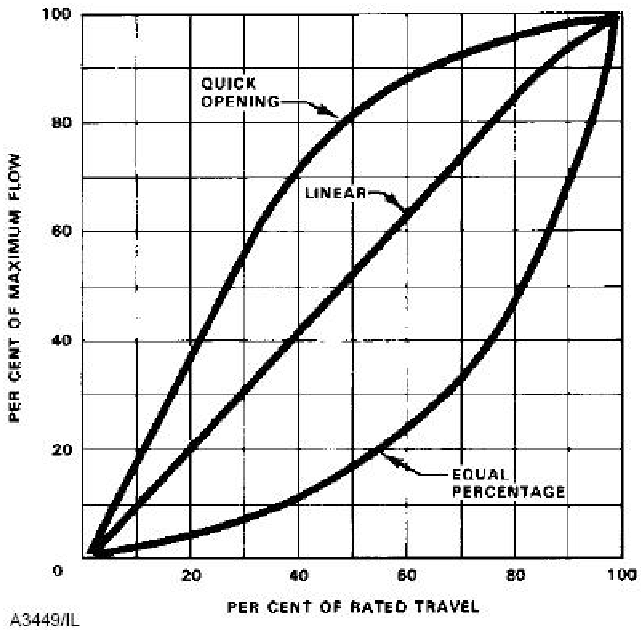

Figure 2.2: Inherent Characteristics Of Valves

seat arrangement causes the difference in valve opening between these valves. The most common characteristics are shown in Fig 2.2 [11]. The percent of flow through the valve is plotted against valve opening, which in the present models, is assumed as a function of disk angular position. The curve is based on constant pressure drop across the valve and the inherent characteristic expressed by C_v is shown in Fig 2.3 for a check valve used in the present model. The maximum and minimum angular position of the disk is 80 and 0 in degree. Then, Eqn 2.8 can be rewritten as

$$T_h = \gamma \Delta H \overline{r} A_v \tag{2.10}$$

in which $\overline{r}$ is the distance from the hinge to the point of application of the average pressure change across the valve, and A_v is the disk area over which ΔH acts. Substitution of all

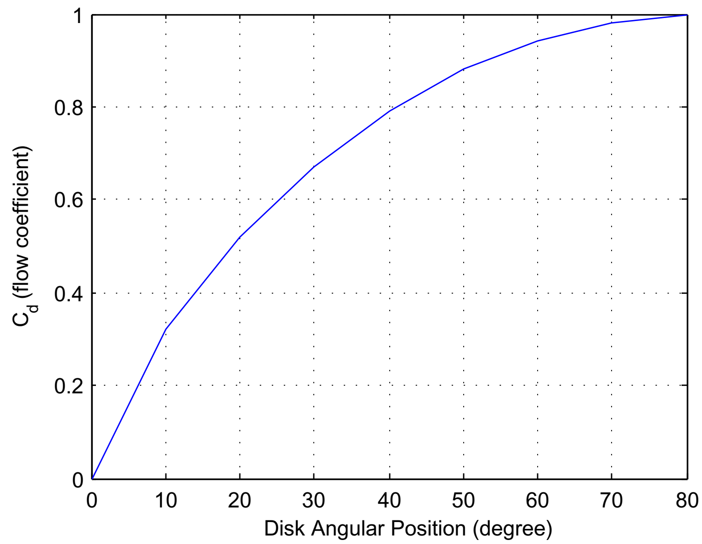

Figure 2.3: Flow Coefficient Used For Present Model

torques into Equation(2.4) gives

$$I\frac{d^2\theta}{dt^2} = W_c r_c \sin\theta + s\theta + \frac{\gamma \overline{r} A_v Q\,|Q|}{2g(C_d A_o)^2} \tag{2.11}$$

Each torque of the equation as described above would be classified into two categories, either the opening torque or closing torque. The opening torque includes the torque due to weight of the rotating disk, T_w, and the external torque due to spring, T_e. The hydraulic torque may be either opening or closing torque depending on the flow direction. The values of each torque is calculated at each time step. Under the steady state condition it is clear that the opening torque is greater than the closing torque. When unsteady state is created in the system, if the opening torque is less than the opening torque, the check valve may accelerate its move toward the close position. The characteristics of valves may be determined, considering how the valves move along with the

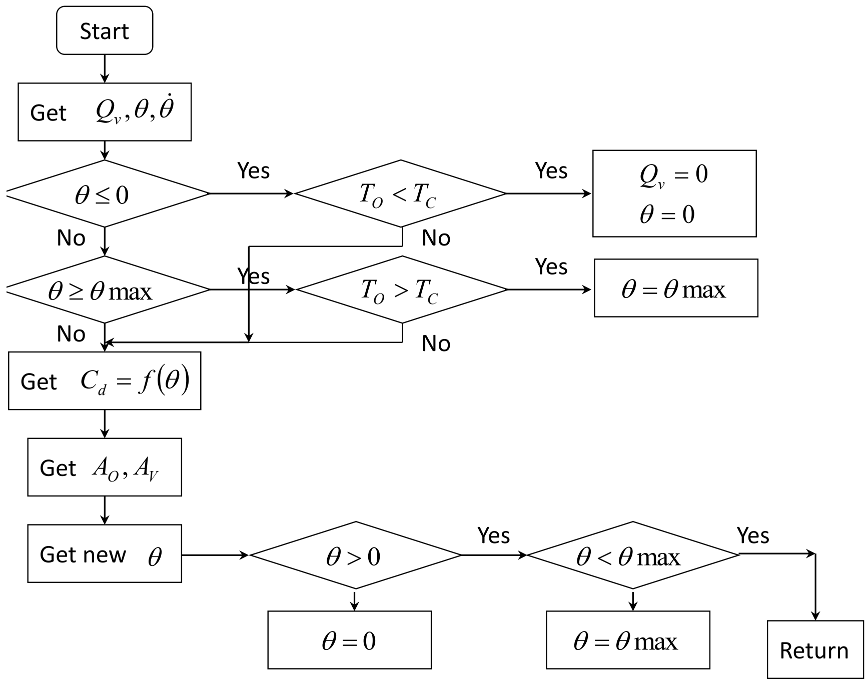

Figure 2.4: Computer Algorithm For Coupling Model

changes in flow conditions. The parameters such as a response time(i.e. quick closing, equal percentage), a closing time, linearity, and so on. The combination of the valve equation and the pipe equations is essential to study the flow-valve interaction. Fig 2.4 represents the flow chart of programming algorithm for the coupling model used in the present study. With given initial values of Q, θ, and $\dot{\theta}$, new θ, and $\dot{\theta}$ can be updated for each time step. Since the response time of the system is rapid, it is necessary to use a higher-order integration scheme in handling the equation. Therefore, the fourth-order Runge-Kutta method is used to solve the differential equation.

Chapter 3

Method of Characteristics

A numerical solution of the governing equations for unsteady pipe flow presented in the previous chapter is introduced in this chapter. Also, various boundary conditions are presented.

3.1 Solution by Method Of Characteristics

The popular method of characteristics is a simple and numerically efficient way of solving the unsteady flow equations. The continuity and momentum equations form a pair of hyperbolic partial differential equations in terms of dependent variables, V and H, and independent variables, x and t. By using the method of characteristics, two partial differential equations can be transformed into the four ordinary differential equations. These equations are then integrated to obtain a finite difference representation of the variables. In the method of characteristics, each boundary and each conduit section are analyzed separately during a time step. This advantage allows a powerful tool particularly for the analysis of systems having complex boundary conditions. The characteristics method is developed in more detail in this section.

The governing equations are summarized again as following:

$$L_1 = \frac{\partial H}{\partial t} + \frac{a^2}{g}\frac{\partial V}{\partial x} = 0 \tag{3.1}$$

$$L_2 = g\frac{\partial H}{\partial x} + \frac{\partial V}{\partial t} + \frac{f}{D}\frac{V\left|V\right|}{2} + k_2\left(\frac{\partial V}{\partial t} - a\frac{\partial V}{\partial x}\right) = 0 \tag{3.2}$$

The momentum equation in Eqn 3.2 is rearranged as

$$L_2 = \left(1 + k_2\right)\frac{\partial V}{\partial t} - ak_2\frac{\partial V}{\partial x} + g\frac{\partial H}{\partial x} + \frac{f}{D}\frac{V\left|V\right|}{2} = 0 \tag{3.3}$$

The transformation of Equation(3.3) by the method of characteristics, multiplied by a linear multiplier λ, gives two pairs of the ordinary differential equations. Now, let's consider the linear combination, $L{=}(g\lambda/a)\,L_1{+}L_2$.

$$\left(1 + k_2\right)\left[\frac{\partial V}{\partial t} + \frac{\left(\lambda - k_2\right)a}{1 + K_2}\frac{\partial V}{\partial x}\right] + \frac{g\lambda}{a}\left(\frac{\partial H}{\partial t} + \frac{a}{\lambda}\frac{\partial H}{\partial x}\right) + \frac{f}{D}\frac{V\left|V\right|}{2} = 0 \tag{3.4}$$

With $H = H(x,t)$ and $V = V(x,t)$, the total derivatives may be written by chain rule, Eqn 3.5 and 3.6, as:

$$\frac{dV}{dt} = \frac{\partial V}{\partial t} + \frac{\partial V}{\partial x}\frac{dx}{dt} \tag{3.5}$$

$$\frac{dH}{dt} = \frac{\partial H}{\partial t} + \frac{\partial H}{\partial x}\frac{dx}{dt} \tag{3.6}$$

Therefore, Eqn 3.4 can be written as:

$$\left(1 + k_2\right)\frac{dV}{dt} + \frac{g\lambda}{a}\frac{dH}{dt} + \frac{fV\left|V\right|}{2D} = 0 \tag{3.7}$$

$$\frac{dx}{dt} = \frac{\left(\lambda - k_2\right)a}{1 + k_2} = \frac{a}{\lambda} \tag{3.8}$$

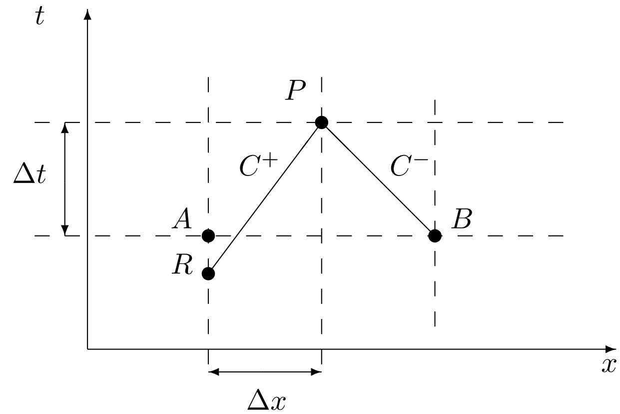

Figure 3.1: Characteristic Lines In x-t Plane

The unknown multiplier can be determined from Eqn 3.8:

$$\lambda = 1 + k_2 \; or \; -1 \tag{3.9}$$

Substitution of these values of λ into Eqn 3.7 leads to two pairs of ordinary differential equations, identified as C^+ and C^- equations.

$$C^+ : \qquad (1+k_2)\frac{dV}{dt} + \frac{g(1+k_2)}{a}\frac{dH}{dt} + \frac{fV\,|V|}{2D} = 0 \tag{3.10}$$

$$\frac{dx}{dt} = \frac{a}{1+k_2} \tag{3.11}$$

$$C^- : \qquad (1+k_2)\frac{dV}{dt} - \frac{g}{a}\frac{dH}{dt} - \frac{fV\,|V|}{2D} = 0 \tag{3.12}$$

$$\frac{dx}{dt} = -a \tag{3.13}$$

Eqn 3.10 and 3.12 are not valid everywhere in the x-t plane. The equations are valid only along the straight lines(if the wave speed, a, is constant) given by Eqn 3.11 and 3.13, respectively. In Fig 3.1, Eqn 3.11 and 3.13 represent two straight lines having slopes $+\frac{1+k_2}{a}$ and $-\frac{1}{a}$. To satisfy these characteristic relations, the x-t grid requires to be chosen to ensure the Courant condition which is:

$$\frac{\Delta t}{\Delta x} \leq \frac{1}{a} \tag{3.14}$$

Once initial conditions and the grid are specified, Eqn 3.10 and 3.12 can be integrated along the C^+ and C^- characteristic lines.

$$C^+ : H_P = C_P - B_P Q_P \tag{3.15}$$

$$C^- : H_P = C_M + B_M Q_P \tag{3.16}$$

in which the coefficients are all known constants when the equations are applied.

$$C_P = H_R + Q_R \left(C_a - R \left| Q_R \right| (1 - \epsilon) \right)$$

$$B_P = C_a + \epsilon R \left| Q_R \right|$$

$$C_M = H_B - Q_B \left((1 + k_2) C_a - R \left| Q_B \right| \right)$$

$$B_M = (1 + k_2)\, C_a$$

$$R = \frac{f \Delta x}{2gDA^2}$$

$$C_a = \frac{a}{gA}$$

$$\epsilon = a \ linearization \ constant$$

The weighting term ϵ influences the friction approximation on the third integral term in Eqn 3.10 and 3.12 without changing the discretization terms such as Δt, Δx, or a. Thus, it provides an excellent way of assessing the sensitivity of a transient simulation to friction values. The term Q_R and H_R can be determined by using linear time line interpolation such as

$$Q_R = Q_A - I_P\left(Q_A - Q_{A'}\right) \tag{3.17}$$

$$H_R = H_A - I_P\left(H_A - H_{A'}\right) \tag{3.18}$$

$$I_P = \sqrt{1 + k_2} - 1 \tag{3.19}$$

and prime indicates the value at previous time step.

By eliminating Q_P in the characteristic equations,

$$H_P = \frac{C_P B_M + C_M B_P}{B_P + B_M} \tag{3.20}$$

$$Q_P = \frac{C_P - C_M}{B_P + B_M} \tag{3.21}$$

The values of H and Q are found at grid intersection points P_2, P_3, ..., P_{N-1} at $j\Delta t$. Then time is incremented by Δt and the procedure is repeated for interior points.

3.2 Boundary Conditions

A number of simple boundary conditions used in the present model are introduced in this section. Also, complex boundary condition such as for a check valve are developed.

3.2.1 Constant-Level Upstream Reservoir

If the volume of reservoir is considerably large, so that the changes in the reservoir level may be small during the time period of interest, the water level in the reservoir can be assumed constant. If the entrance losses as well as the velocity head are negligible, then

$$H_P(1,1) = H_{res}$$
$$Q_P(1,1) = \left(H_P(1,1) - C_M(1,2)\right)/B_M(1,2) \tag{3.22}$$

For the present model, $Q_P(1,1)$ is given as a known function of time (e.g., control valve at upstream end). Hence, $H_P(1,1)$ is calculated from Eqn 3.22.

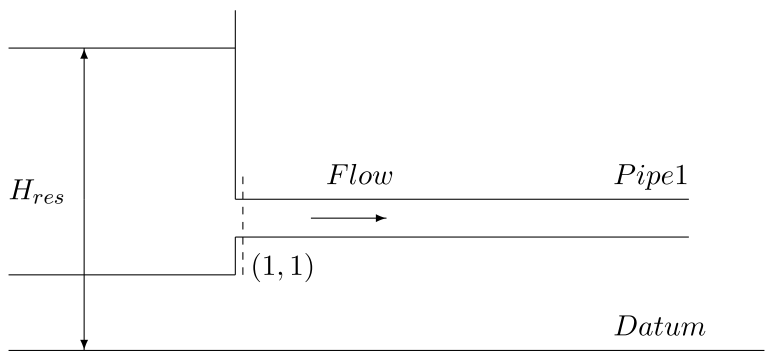

Figure 3.2: Constant-Level Upstream Reservoir

3.2.2 Series Junction

A series junction is a junction of two conduits have different diameters, wall thicknesses, wall materials, and/or friction factors. A simple junction connecting two pipes is shown in Fig 3.3. If the difference in the velocity heads at sections(i, N) and $(i+1, 1)$ and the head losses at the junction are negligible, it can be written from the energy equation and the continuity.

$$H_P(i,N) = H_P(i+1,1) \tag{3.23}$$

$$Q_P(i,N) = Q_P(i+1,1) \tag{3.24}$$

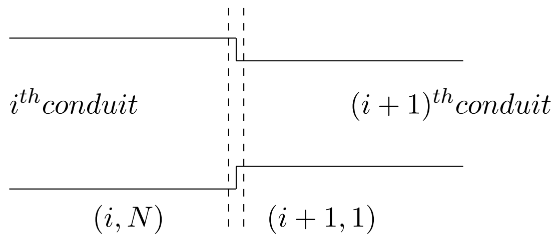

Figure 3.3: Series Junction

From the characteristic equation for each conduit it is followed:

$$H_P(i,N) = C_P(i,N-1) - B_P(i,N-1)Q_P(i,N) \tag{3.25}$$

$$H_P(i+1,1) = C_M(i+2,2) + B_M(i+1,2)Q_P(i+1,1) \tag{3.26}$$

It follows from Equation(3.23) through Equation(3.26) that

$$Q_P(i,N) = \frac{C_P(i,N-1) - C_M(i+1,2)}{B_M(i+1,2) + B_P(i,N-1)} \tag{3.27}$$

$$Q_P(i+1,1) = Q_P(i,N) \tag{3.28}$$

3.2.3 Valve At Downstream End

At the pipe outlet, the continuity condition at the downstream end requires that $Q_P = Q_{out}$. If Q_P is given as a function of time, from the C^+ equation, it follow that

$$H_P = C_P - B_P Q_P \tag{3.29}$$

3.2.4 Backflow Prevention Assembly

A Backflow prevention assembly is a mechanical device located within a given pipeline, usually as close as possible to the drinking water service connection. Ideal backflow prevention assemblies close at an instant the flow reverses. However, more realistically, some level of reversal flow usually occurs because of the inertia of the system. This instantaneous stoppage of the reverse flow causes the corresponding pressure rise called valve slam. Fig (3.4) illustrates a schematic of a single check valve with nodes a and b as the interconnecting junctions on both sides of the internal valve.

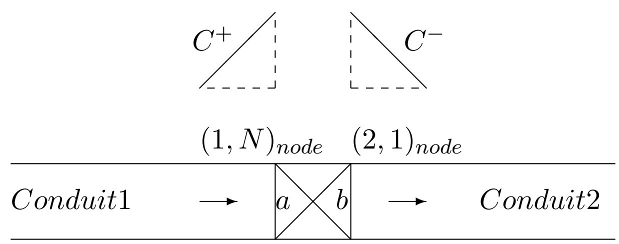

Figure 3.4: A Schematic of Check Valve Between Two Pipes

For positive flow with $H_{1,N} = H_a$ and $H_{2,1} = H_b$, the valve equation is

$$\begin{aligned} Q_{1,N} &= Q_{2,1} = Q_v \\ &= C_d A_o \sqrt{2g\Delta H} \\ &= C_d A_o \sqrt{2g\left(H_a - H_b\right)} \end{aligned} \tag{3.30}$$

$$\begin{aligned} \Longrightarrow Q_v^2 &= \left(C_d A_o\right)^2 (2g) \left(H_a - H_b\right) \\ &= \left(C_d A_o\right)^2 (2g) \left[\left(C_{p1} - C_{M2}\right) - \left(B_{P1} + B_{M2}\right) Q_v\right] \end{aligned}$$

$$Q_v^2 + \left(C_d A_o\right)^2 (2g) \left(B_{P1} + B_{M2}\right) Q_v - \left(C_d A_o\right)^2 (2g) \left(C_{p1} - C_{M2}\right) = 0 \tag{3.31}$$

A quadratic equation to solve Equation(3.31) is given:

$$Q_v = -C_v \left(B_{P1} + B_{M2}\right) + \sqrt{C_v^2 \left(B_{P1} + B_{M2}\right)^2 + 2C_v \left(C_{P1} - C_{M2}\right)} \tag{3.32}$$

where $C_v = C_d^2 A_o^2 g$. Similarly for the negative flow, Q_v is calculated by using the following equation.

$$Q_v = C_v \left(B_{P1} + B_{M2}\right) - \sqrt{C_v^2 \left(B_{P1} + B_{M2}\right)^2 - 2C_v \left(C_{P1} - C_{M2}\right)} \tag{3.33}$$

It is noted that a negative flow is possible only if $C_{P1} - C_{M2} < 0$. Hence Equation(3.32) is used if $C_{P1} - C_{M2} >= 0$, and Eqn 3.33 is used if $C_{P1} - C_{M2} < 0$. Once the flow is known, the characteristic equations are used to obtain the hydraulic heads for each section a and b. The backflow prevention assembly with a single check valve inside used in the computer simulations is modeled for three different types:

- An ideal valve type
- undamped type
- damped type

The model for an ideal valve does not allow a reversed flow through the assembly (Q_v is always positive or zero) while other models may allow a backflow in the system (Q_v is either positive or negative).

3.3 Coupling Modeling

The combination of the valve equations and the pipe equations is essential to study the fluid-valve interaction and to study the dynamic motion of check valves during transient events. The pipe equations include the continuity and momentum equations introduced in Eqn 2.1 and 2.3. The valve equations include the moment-of-momentum equation of the check disk and the valve equation introduced in Eqn 2.11 and 3.30, respectively. At each time step, the coupling model starts with initial disk angle positon, θ, and initial disk angular velocity, $\dot{\theta}$. The flow coefficient, C_d, is given for a specific valve type and is linearly interpolated. With Q_v, θ, and $\dot{\theta}$, the moment of momentum equation is solved numerically by the Runge-Kutta 4^{th} method to estimate new values of ${Q_v}'$, θ', and $\dot{\theta}'$. The prime represent the values of variables at the next time step. And coefficients are updated using new variables of ${Q_v}'$, θ', and $\dot{\theta}'$.

Chapter 4

Experiments

Now two different sets of experimental records are presented in this chapter. The data collected from the experiments will be used in the next chapter to compare with the numerical simulations in an effort to determine varying coefficients for a specific system. Case 1 represents a simple valve-pipeline-valve system without a backflow prevention assembly installed. The comparisons are presented for case 1, one with quasi-steady friction only and the second with the unsteady friction coefficient, K_2, included to simulate the unsteady friction effects during rapid transient events. Case 2 represents a system within which a backflow prevention assembly is installed. The comparison between two different cases, one with a backflow prevention assembly and the second without backflow prevention assembly.

4.1 Experimental Setup

As illustrated in Fig 4.1, a 84.73 m long galvanized iron steel pipe with 0.0525 m in diameter was installed for experiments. In order to reduce the occupied space the pipeline was set up bent using ten 90-degree-elbow fittings. The system was fed from upstream main pipeline where the line pressure is normally maintained to 150 $lbf/in^2[psi](\approx 105$ meter of water). Two control valves of ball valve type were installed at each end of pipelines. Both control valves are then closed simultaneously by manual operation to create the transient flow. A positive pressure wave is created at downstream end of pipeline and then it propagates to upstream. A negative pressure wave, by contrast, is created at upstream end of pipeline, propagating to downstream. The line pressure under the steady-state flow condition was able to be controlled by the pressure-reducing valve installed prior to the upstream control valve. In both Case 1 and Case 2, the initial conditions are kept the same as soon as possible, except for the installation of a backflow prevention assembly for the system. Pressure time history data were measured by two pressure sensors. Two pressure transducers were embedded at location of 20.4 m and 63.4 m measured from the upstream end. For the measurement of the flow rate, a pair of flow meters was used. To regulate the line pressure of the system a pressure reducing valve is installed at the upstream end just before the upstream control valve. Many tests are performed varying the line pressure by adjusting the pressure valve. The physical properties of the pipe material and water are summarized in Table 4.1.

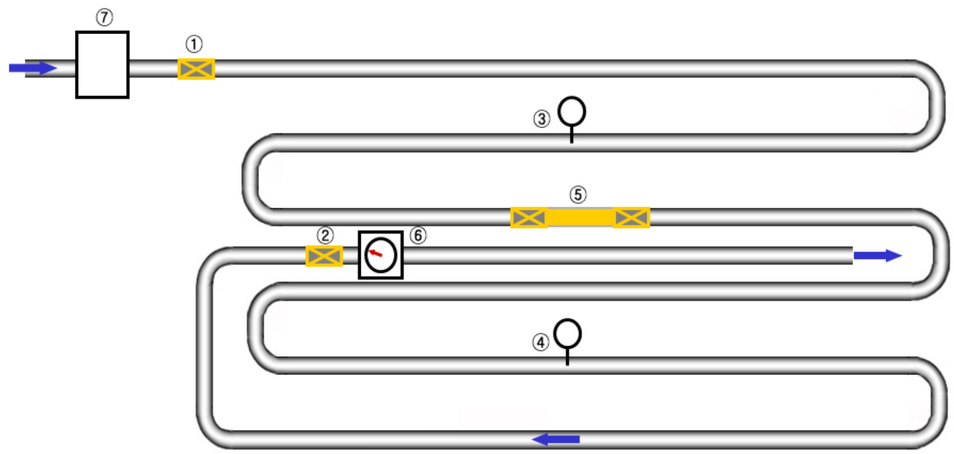

(1) Upstream Shut-off Valve (2) Downstream Shut-off Valve (3) Transducer#1

(4) Transducer#2 (5) Backflow Preventer (6) Flow Meter (7) Pressure Regulator

Figure 4.1: Testing Loop

According to the evaluation of total head losses by H.J. Kwon [10], the total head loss of the system is a summation of the frictional loss and the minor losses for the various items contained in the system. The effect of the minor losses to the system's total head loss is significant in the region of lower Reynolds number, used in the present experiment.

Although many cases of experiments have been performed during the study, two cases will be selected to represent two different pipeline system, equipped with/or without a hydraulic device such as backflow prevention assemblies. For case 2, the location of a backflow prevention assembly is measured 35.8 m from the upstream end.

Property	Value
Total Length of Pipe	84.7344 m
Diameter of Pipe	5.25×10^{-2} m
Thickness of Pipe	3.912×10^{-3} m
Number of Elbow pipe fittings	10
Bulk Modulus of Pipe Material	2.07 Gpa
Young's Modulus of Pipe Material	206.86 Gpa
Density of Water	$999.1845\, kg/m^3$
Kinematic Viscosity of Water	$1.13 \times 10^{-6}\ m^2/sec$

Table 4.1: Physical Properties Of System

4.2 Case 1: Without a Backflow Prevention Assembly

A set of experimental data for this case was obtained for a simple valve-pipeline-valve system with the following characteristics: The line pressure at the upstream end under the steady state condition was simply measured by a line pressure gauge. The line pressure at upstream is maintained at 84.3683 m and the flow rate before the control valves are close is maintained at $7.886 \times 10^{-4}\, m^3/sec$. Since the shut-off valves at both end were controlled manually, the detailed characteristics of closing or opening mechanism is not available. Therefore, the changes in flow rate at upstream and downstream are given as a function of time, $Q_{up} = f_1(t)$ and $Q_{down} = f_2(t)$. It was estimated from the measured data that the upstream shut-off valve started closing at 0.701 sec and completed closing at 0.732 sec and the downstream shut-off valve started closing at 0.714 sec and completely closed at 0.7355 sec. By linear interpolation, the changes in Q are given as $Q_{up} = -0.0254t + 0.0186$ and $Q_{down} = -0.0367t + 0.027$. These linear equations for the control valves will be used for boundary conditions of the computer simulation.

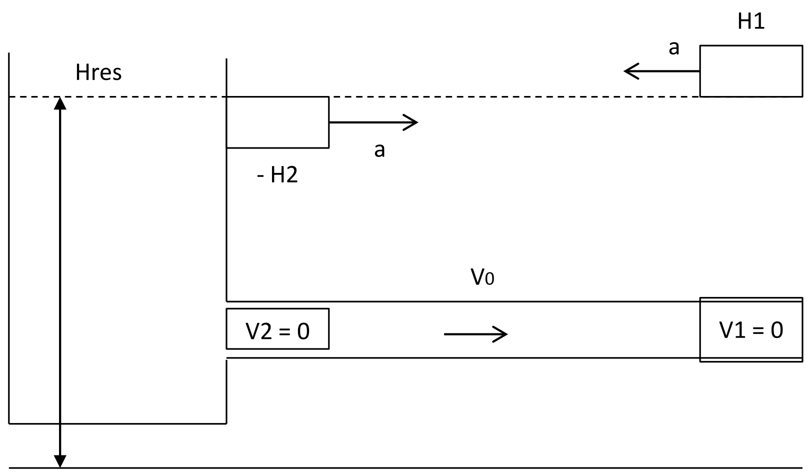

(a) $0 \leq t \leq L/a$

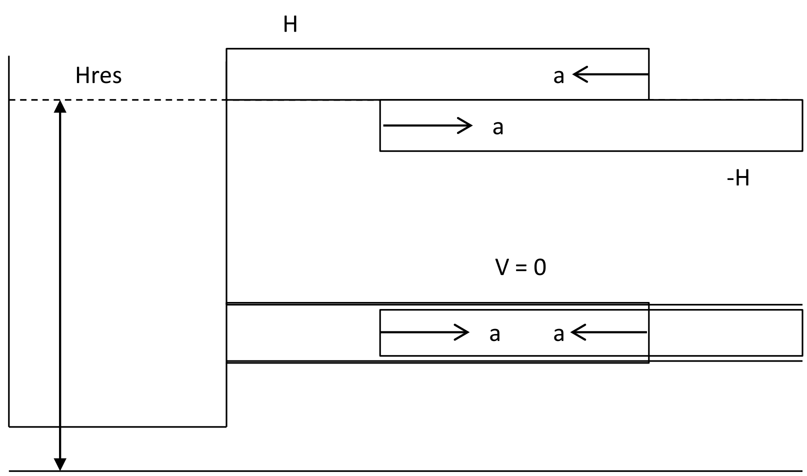

(b) $L/a \leq t \leq 2L/a$

Figure 4.2: Sequence of Water Hammers Occurred in System

Fig 4.2 describes the sequence of water hammer event occurring in the system after the shut-off valves at both ends close at the same time. At the instant of that the downstream valve closes, the fluid nearest the upstream control valve is compressed creating an extra pressure, ΔH. The high pressure moves upstream at the wave speed of a as a positive wave. Similarly, a negative wave that is created by the upstream valve closure moves downstream at the same wave speed. When two opposite waves rencounter in the middle of pipe, there may be extra energy losses due to friction. After the instant of encounter between two waves, the velocity of fluid is everywhere zero. At the instant of L/a, the waves arrive at the ends of pipe and bound back to the backward direction. Since the valves completely close, the pressure therefore drops to $H_o - \Delta H$ at the upstream end and jumps to $H_o + \Delta H$ at the downstream end. The reflected waves reach at the ends of pipe at $t = 2L/a$. This process is repeated every $2L/a$. The action of friction between fluid and pipe wall damps out the oscillation of the waves and eventually causes the waves to come to rest permanently.

Fig 4.3 and 4.6 are the pressure time history measured at the upstream and downstream locations, respectively. The figures clearly show that two pressure waves are generated from upstream and downstream ends and they oscillate with the period of $2L/a$. The magnitude of the pressure wave is quickly reduced due to great energy losses mainly by friction. Evaluation of damping is discussed in detail in the next chapter 5.

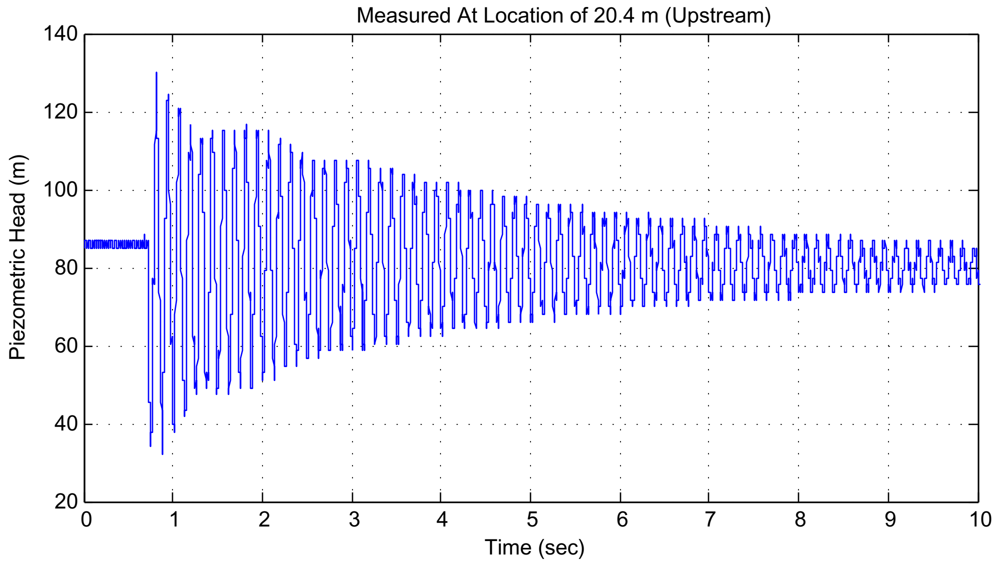

Figure 4.3: Case 1 Pressure Time History At Upstream For $0 \leq t \leq 10$

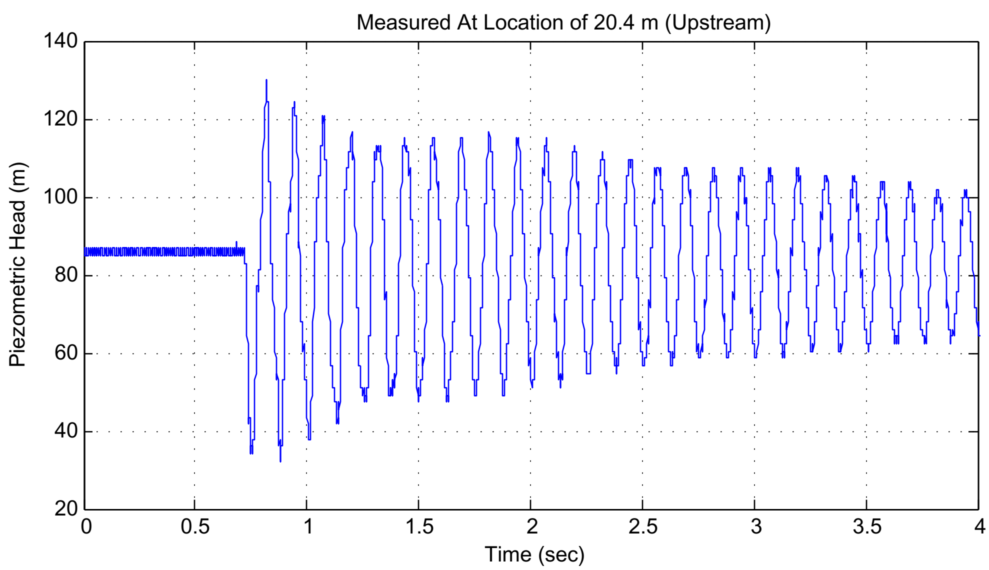

Figure 4.4: Case 1 Pressure Time History At Upstream For $0 \leq t \leq 4$

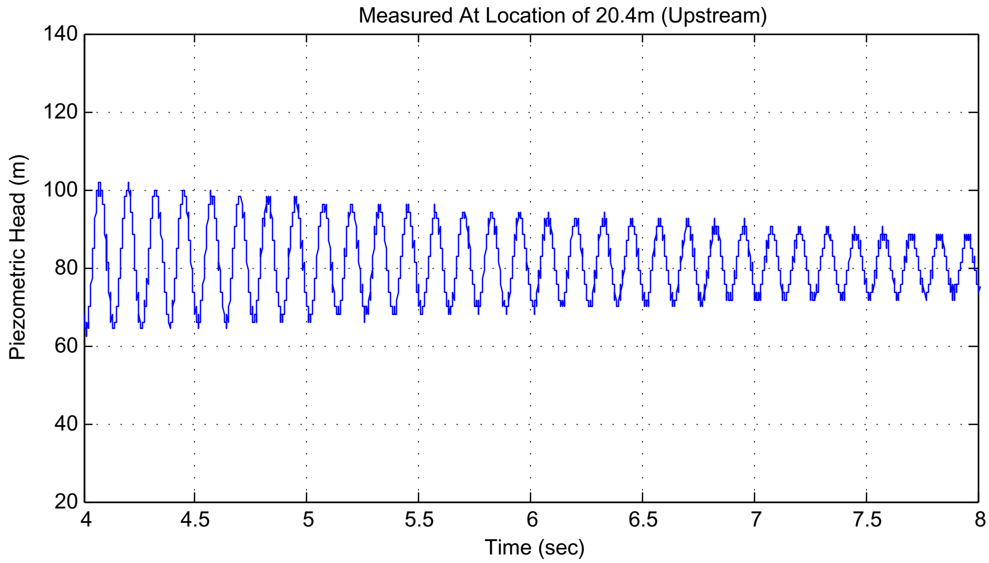

Figure 4.5: Case 1 Pressure Time History At Upstream For $4 \leq t \leq 8$

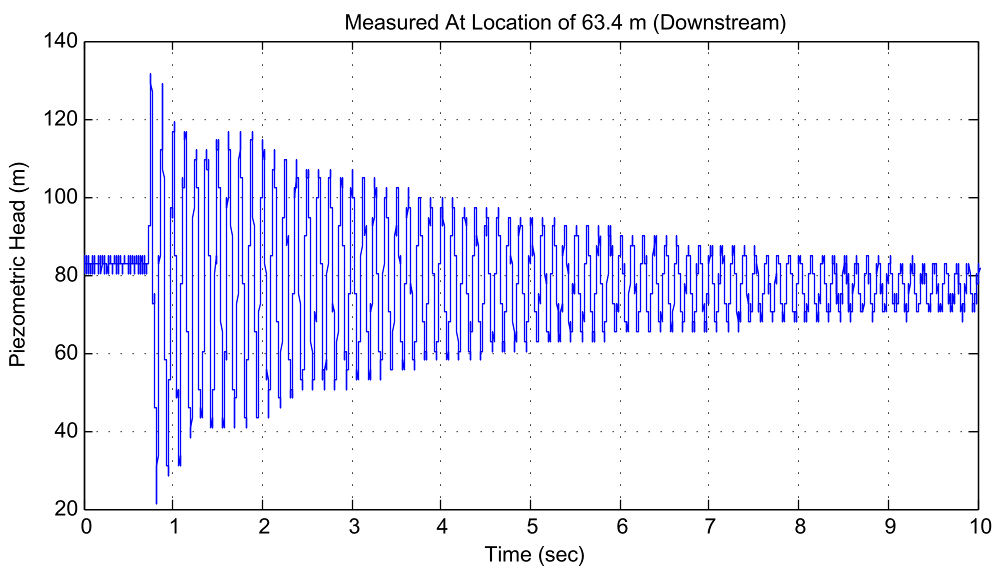

Figure 4.6: Case 1 Pressure Time History At Downstream For $0 \leq t \leq 10$

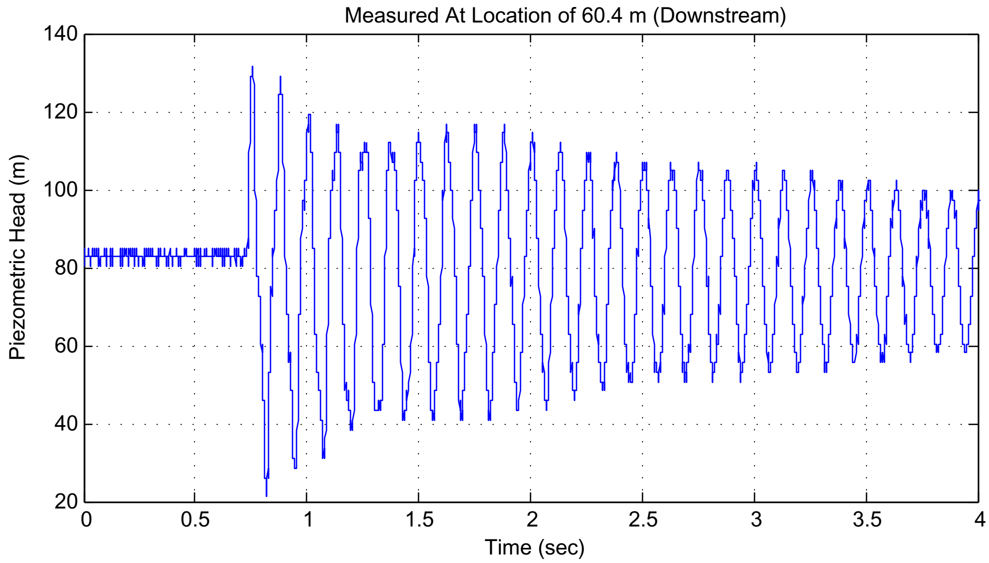

Figure 4.7: Case 1 Pressure Time History At Downstream For $0 \leq t \leq 4$

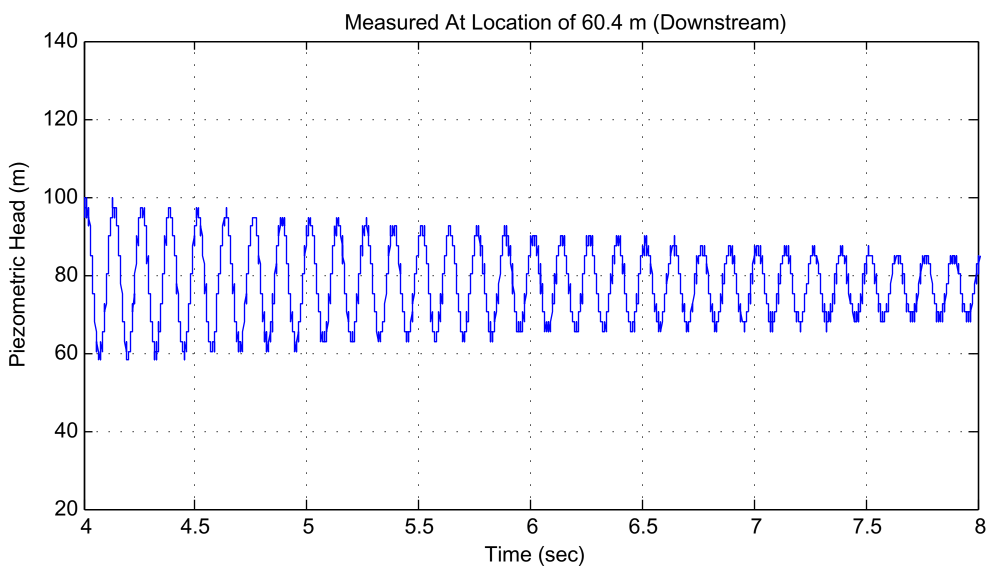

Figure 4.8: Case 1 Pressure Time History At Downstream For $4 \leq t \leq 8$

4.3 Case 2: With A Backflow Prevention Assembly

This experiment is designed to find the effects of water hammer on a backflow prevention assembly and the interactions between the transient flow conditions and an assembly installed in the system. A backflow prevention assembly with a single internal check valve is installed at location of 35.8 m away from the upstream end of pipeline. Similarly to Case 1, pressure waves were created from both end by a sudden closure of both shut-off valves. The line pressure at upstream is maintained at 84.2 m and the flow rate before the control valves are close is maintained at $7.886 \times 10^{-4}\, m^3/sec$. It was shown that the upstream shut-off valve started closing at 0.714 sec and completed closing at 0.737 sec and the closing time of the valve is 0.023 second. The downstream shut-off valve started closing at 0.712 sec and completed closing in 0.027 sec. The experiment conditions for each case are summarized in Table 4.2 and the comparison plot of two cases is presented in Fig 4.18. As seen in Fig 4.18, the response of the system with a backflow prevention assembly is more complex than one of just a simple system. The first peak of two different cases correspond very closely until the backflow prevention assembly is closed. It is noted that with the nearly same flow condition and operation condition, same pressure waves must be created and then moved in the same physical pattern until other hydraulic devices like a backflow prevention assembly in this study, interacts with the flow in the system. After the first peak, the oscillation of the downstream transient continues with a time increment of $4L/a$, where L represents the distance from the downstream end to the backflow prevention assembly location and a represents the wave speed. Once the internal check valve is closed, the pipeline is divided into two sections where are distinguished from dynamic behavior. This experiment clearly shows the occurrence of a check valve slam resulting from a sudden closure of the internal check disk and the fluid-valve interaction during transient events. In Figs 4.9 and 4.12, experimental results for a backflow prevention assembly installed in the middle of the test pipeline are presented.

Information	Case 1	Case 2
Line Pressure Head (m)	84.3683	84.2
Steady-State Discharge Rate (m^3/s)	0.0007571	0.0007571
Wave Speed (m/s)	1367.2	1367.2
Closing Time of SOV Upstream (sec)	0.031	0.023
Closing Time of SOV Downstream (sec)	0.0245	0.027

Table 4.2: Summary of Flow Conditions For Cases

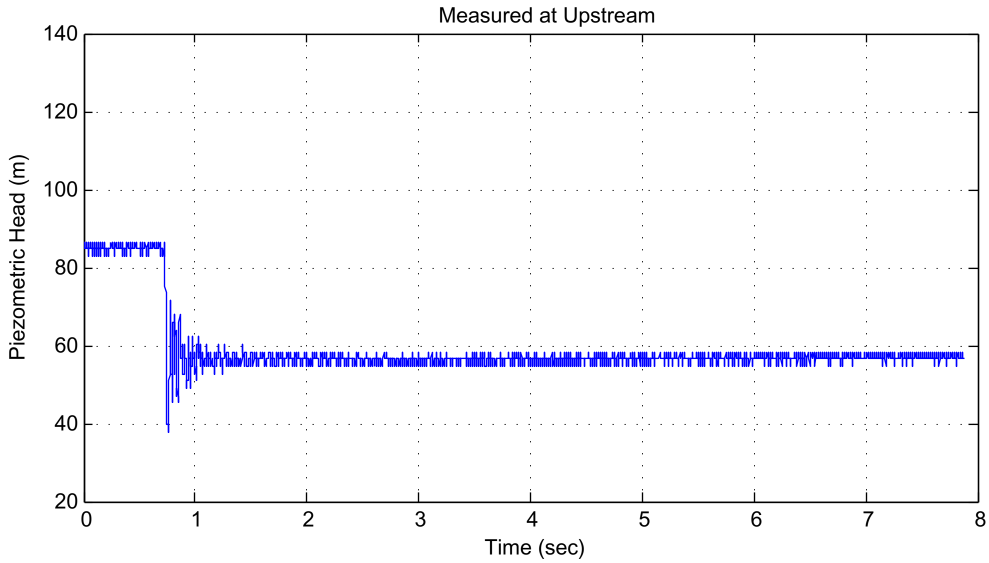

Figure 4.9: Case 2 Pressure Time History At Upstream For $0 \leq t \leq 8$

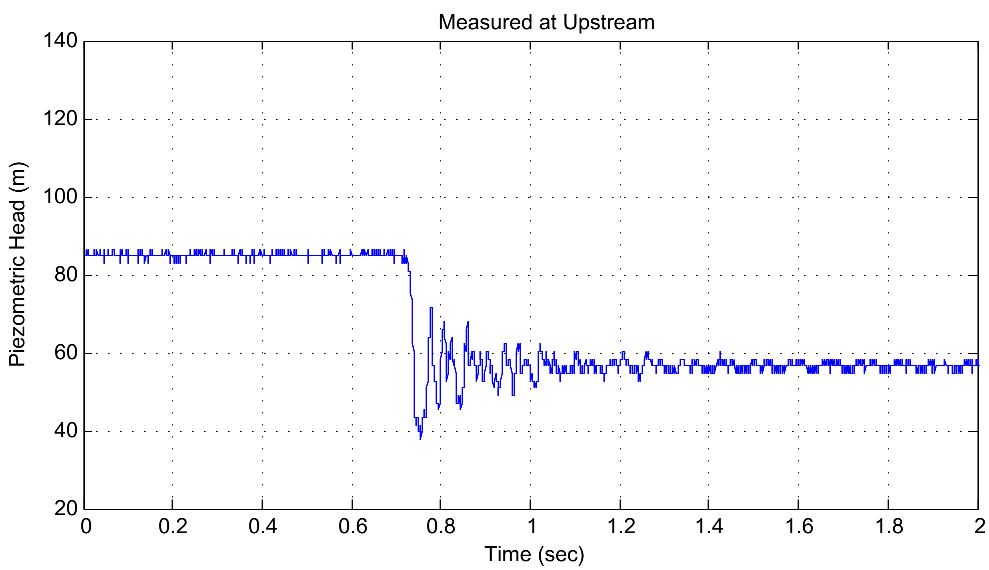

Figure 4.10: Case 2 Pressure Time History At Upstream For $0 \leq t \leq 2$

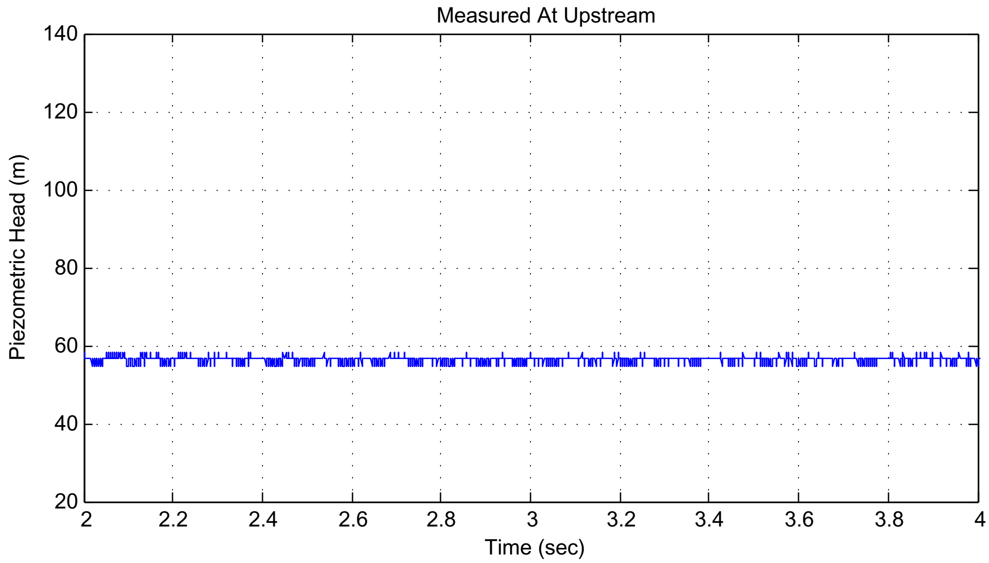

Figure 4.11: Case 2 Pressure Time History At Upstream For $2 \leq t \leq 4$

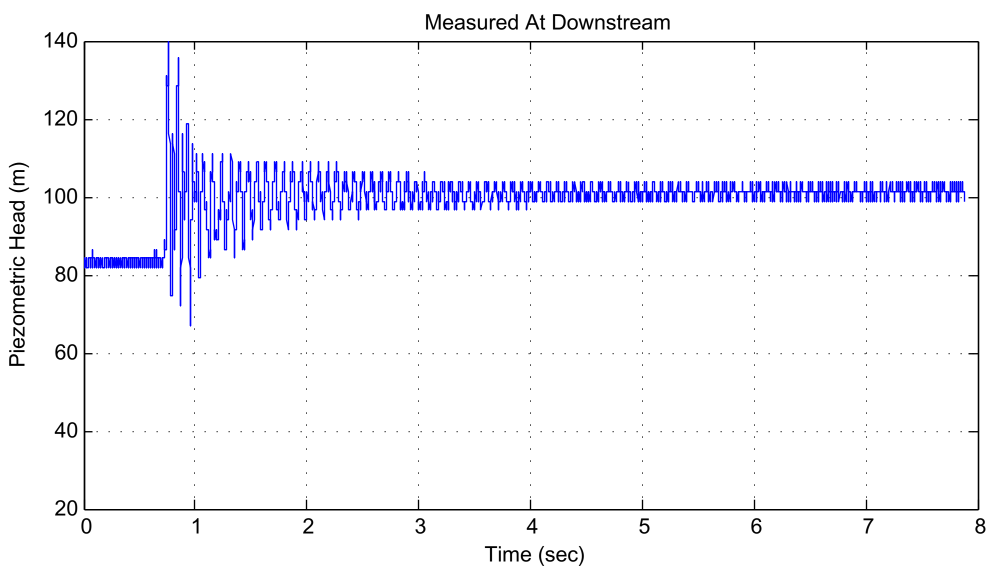

Figure 4.12: Case 2 Pressure Time History At Downstream For $0 \leq t \leq 8$

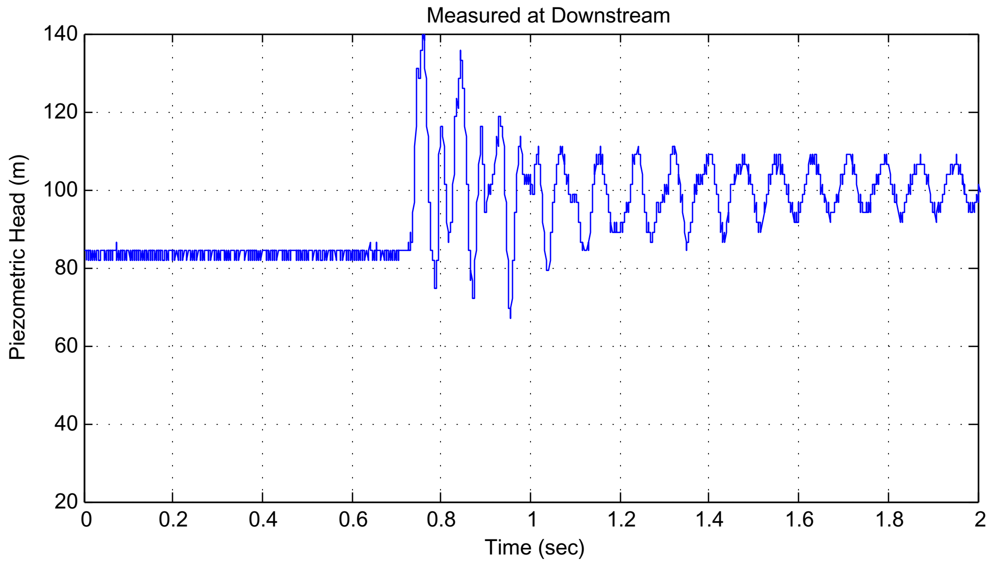

Figure 4.13: Case 2 Pressure Time History At Downstream For $0 \leq t \leq 2$

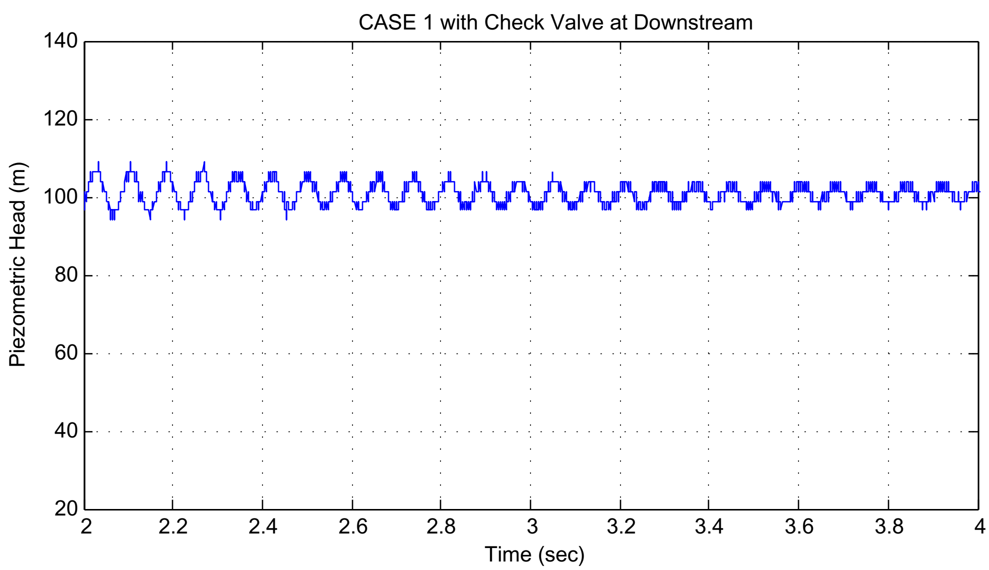

Figure 4.14: Case 2 Pressure Time History At Downstream For $2 \leq t \leq 4$

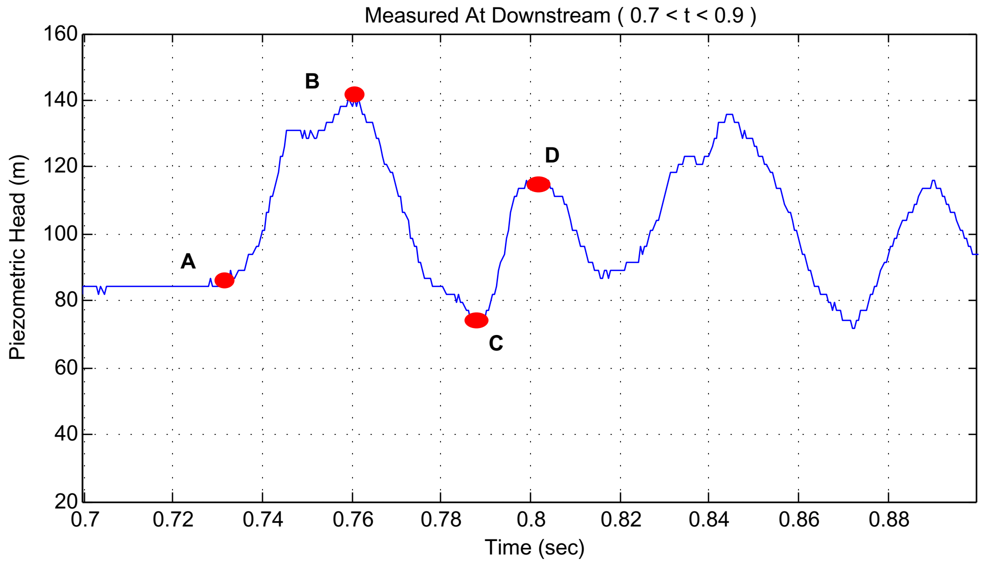

Figure 4.15: Case 2 Pressure At Downstream for $0.7 \leq t \leq 0.9$

As shown more in Fig 4.15, the check valve slam phenomenon is observed from this experiment. Point A corresponds to the closing of the downstream control valve, and is the start of the deceleration of the flow at the backflow prevention assembly. At point B the control valve completes closing and then the internal check valve continues to close from Point B to Point C. The maximum reverse flow is established at Point C and the valve disk strikes the seat causing slam and another water hammer within the downstream region. Then the pressure wave created by a valve slam oscillates back and forth. It is also noted that the energy losses for this case is much larger than those for case 1. This damping effects may be resulted from the interaction between the motion of an internal check valve and flow conditions.

4.4 Comparison of Measured Data Between Case 1 and Case 2

Fig 4.16 and Fig 4.17 present the pressure time histories at the upstream region and Fig 4.18 and Fig 4.19 present the pressure time histories at the downstream region after the shut-off valves close simultaneously. The oscillations in pressure occur quickly being constrained within certain bounds, diminish rapidly with time, and finally reach to another steady states. It is necessary to re-examine the importance of the role that backflow prevention assemblies play during the transient event. The pressure head at the upstream in Case 1 is reduced by 50 m (from 84 to 34) in 0.02 seconds and bounds up to 130 m, the maximum. The range (maximum minus minimum) of pressure head is about 96 m. The maximum pressure head in Case 2, on the other hand, is 72 m, resulting in the range of 38 m. Considering the pressure heads at the downstream region, Case 1 shows the pressure range of 109 m (from 130 to 21) while Case 2 shows the range of 66 m (from 140 to 74). Local flow separation caused by the motion mechanism of backflow prevention assemblies during the transients have the biggest influence on energy dissipation particularly for the initial time of the transient event. It is clearly seen in Figs 4.16and 4.18 that the energy losses in the upstream region is much greater than the energy losses in the downstream region.

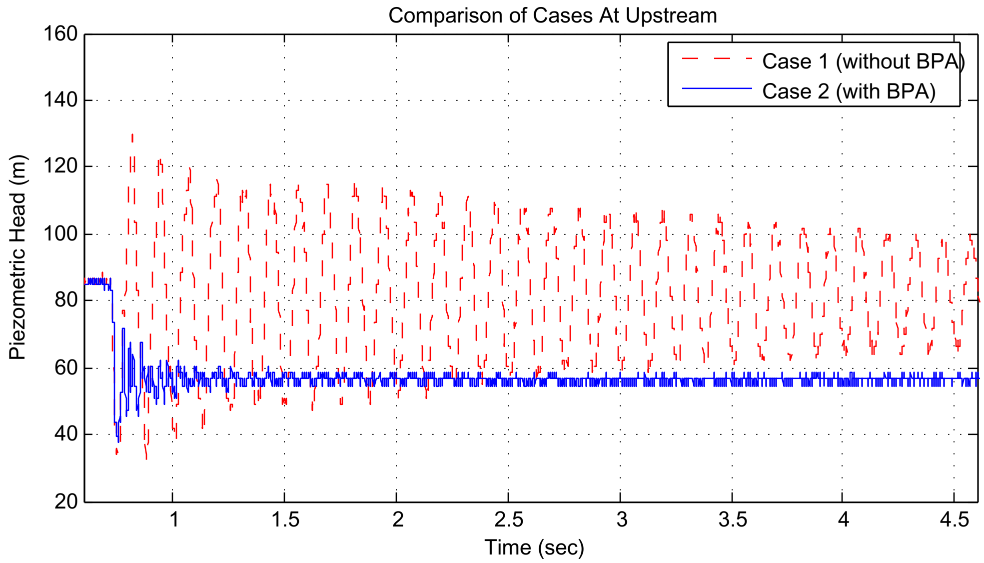

Figure 4.16: Comparison of Two Cases at Upstream for $0.6 \leq t \leq 4.6$

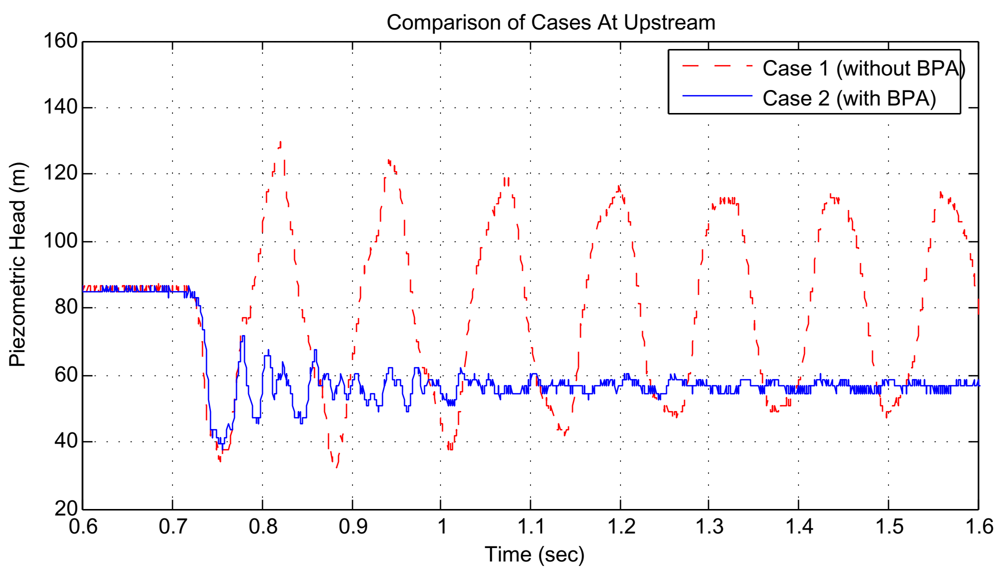

Figure 4.17: Comparison of Two Cases at Upstream for $0.6 \leq t \leq 1.6$

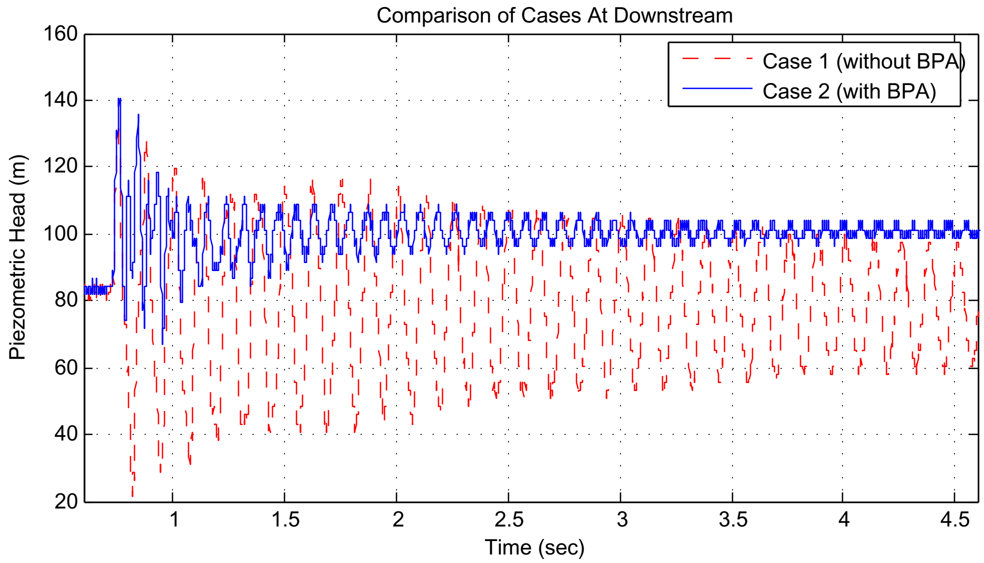

Figure 4.18: Comparison of Two Cases at Downstream for $0.6 \leq t \leq 4.6$

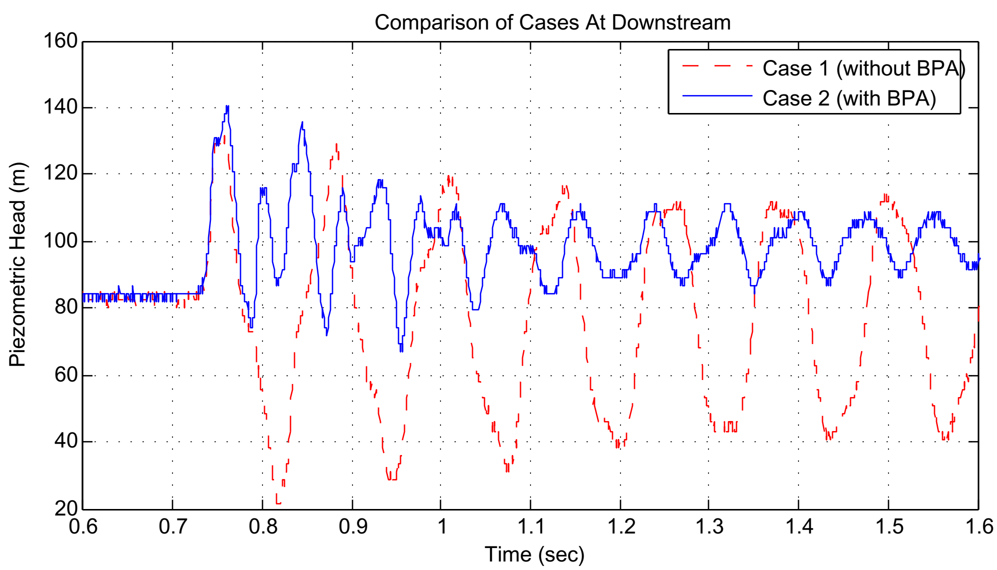

Figure 4.19: Comparison of Two Cases at Downstream for $0.6 \leq t \leq 1.6$

Information	Upstream Region	Downstream Region
Initial Pressure Head at t = 0	84 m	84 m
Range of Pressure difference in Case 1	96 m	109 m
Range of Pressure difference in Case 2	38 m	66 m
Percentage of Reduction	60.4 %	39.4 %

Table 4.3: Summary of Pressure Reduction Rates by Backflow Preventer

As shown in Table 4.3, the backflow prevention assembly reduces the pressure ranges (which defined as maximum minus minimum value) by 60.4 percent and 39.4 percent for the upstream and downstream wave respectively. The experimental result shows that backflow prevention assembly in general acts as a damper to the excessive pressure wave created in the pipe system during the transient.

Chapter 5

Simulation Results and Discussion

The computer simulation results are presented in this chapter. First, the computer simulation results are obtained by using both the quasi-steady 1D model and unsteady friction 1D model for Case 1 without a backflow prevention assembly. Verification of the validity of the numerical models is then performed by comparing the numerical results with experimental data. The unsteady friction 1D model is later expanded to incorporate with the coupling model in order to solve for Case 2. The comparison of the computer results with the experimental data for Case 2, verify the present model's validation for the rapid transient flow in the water distribution pipe system.

5.1 Selection of F_T and k_2

The equivalent head loss coefficient, F_T has been used to replace with the Darcy-Weisbach friction coefficient for calculation to represent the total head losses due to not only friction but minor losses. Because of the unique feature of the experimental piping system, the energy losses due to minor-loss items could not be neglected. Therefore, a new friction coefficient must be chosen with much greater value than the Darcy-Weisbach friction coefficient. The value of F_T was finalized to 0.3 by trial-and-error until the agreement shown in the figures was obtained. It is verified from these results that the agreement on the water hammer wave attenuation between the measured data and the quasi-steady models gets better as the equivalent head loss coefficient increases as shown from Fig 5.1 through Fig 5.6. Also, the value of k_2 used for the unsteady friction model was chosen by trial-and-error until the agreement shown in the figures was obtained while the value of the steady friction coefficient was fixed to 0.3 for Case 1. The k_2 values used for Case 1 and Case 2 are 0.045 and 0.4 respectively. The value selected for k_2 was held as a constant value during computing process. Parameters used for computer simulations are summarized in Table 5.1.

5.2 Verification of Models: Case 1

The first attempt with the quasi-steady model is made with different friction coefficients to simulate for Case 1. As seen in Figs 5.1,5.2, and 5.3, the greater the friction coefficient is, the greater the damping effect becomes. Fig 5.7 shows the experimental record at the location of downstream transducer together with simulation results by the quasi-steady friction model for Case 1. Fig 5.7a, shows a good agreement over the first ten oscillatory periods of time. The decay rate with $F_T = 0.3$ is in good agreement with the recorded data. However, for the long-term period of time after two second the computed pressure oscillation appears to be slightly faster. This result shows the inconsistency

Parameters	Quasi-Steady 1D	Unsteady Friction 1D
Number of Pipes	1	2
Increment of x (Δx)	0.6725 m	0.6758 m, 0.6701 m
Increment of t (Δt)	0.0005 sec	0.00049
Number of Nodes	127	53, 75
Duration of Computation	10 sec	8 sec
Equivalent Friction Factor, F_T	0.3	0.3
k_2	NA	$0 \leq k_2 < 1.0$
ϵ	NA	$0 \leq \epsilon \leq 1.0$

Table 5.1: Input Parameters Used In Simulation

in the assumption of the classical water hammer theory that the water hammer waves propagate at a constant speed. A local vapour cavity formed at shut-off valves may influence on the small changes in the wave speed.

Fig 5.8 shows the experimental record at the same location of downstream transducer together with simulation results by the unsteady friction model with $F_T = 0.3$ and $k_2 = 0.045$ over 6 seconds. Both the oscillatory period and the decay rate agree quite well with the experiment record. The numerical result by using the unsteady friction model in the method of characteristics provides the reasonable result, especially for a long-term oscillatory periods.

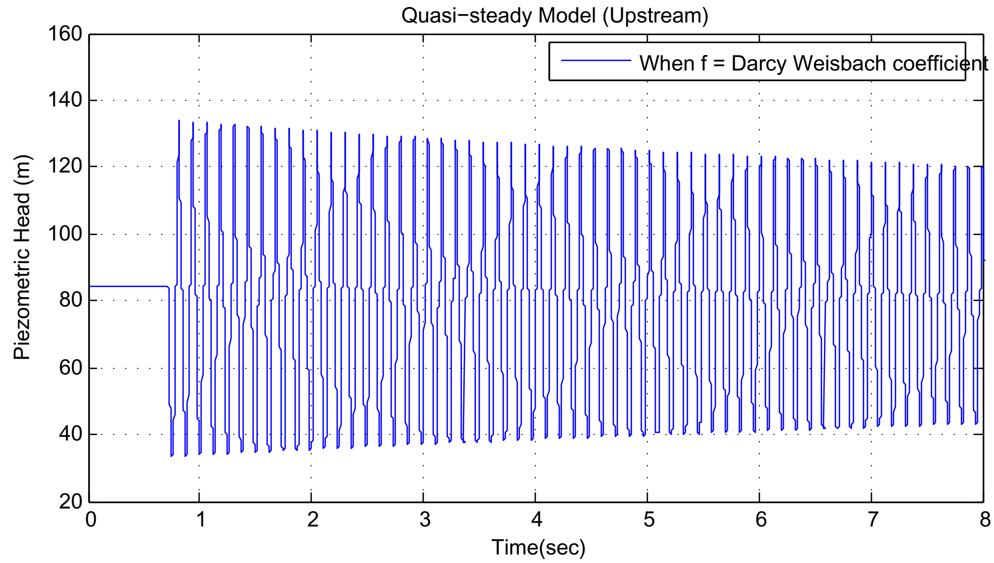

Figure 5.1: Quasi-steady Model with f = Darcy-Weisbach friction coefficient for $0 \leq t \leq 8$

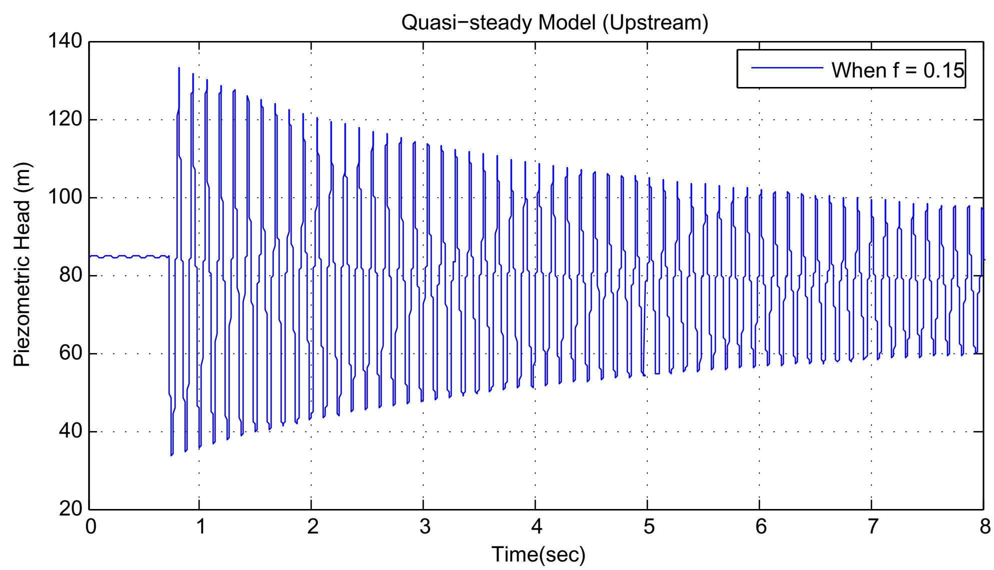

Figure 5.2: Quasi-steady Model with f = 0.15 for $0 \leq t \leq 8$

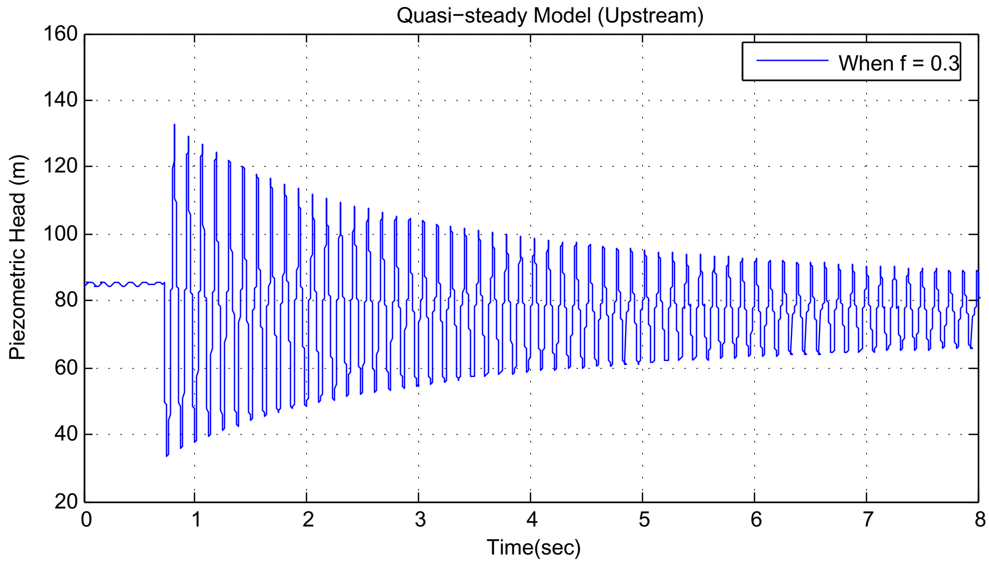

Figure 5.3: Quasi-steady Model with f = 0.3 for $0 \leq t \leq 8$

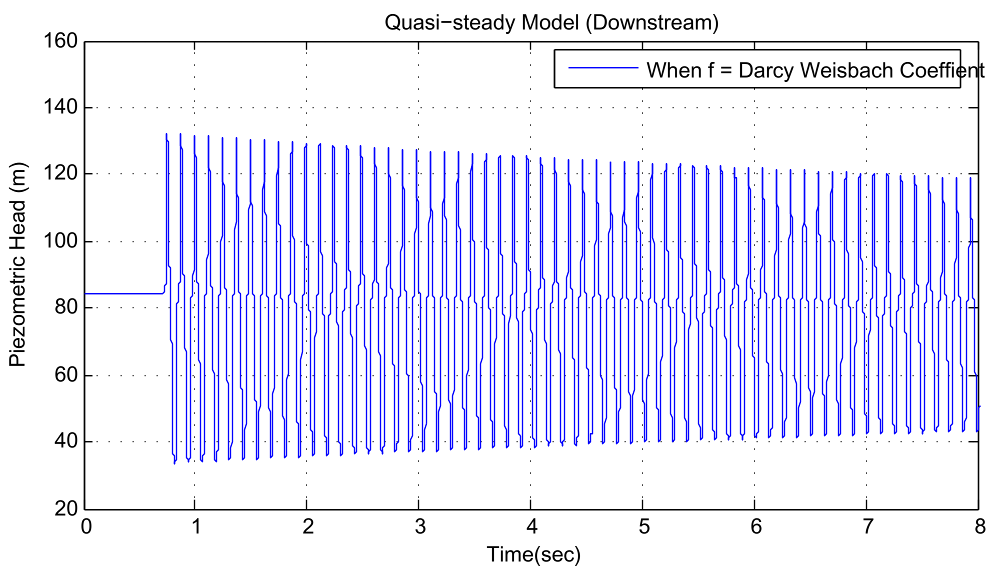

Figure 5.4: Quasi-steady Model with f = Darcy-Weisbach friction coefficient for $0 \leq t \leq 8$

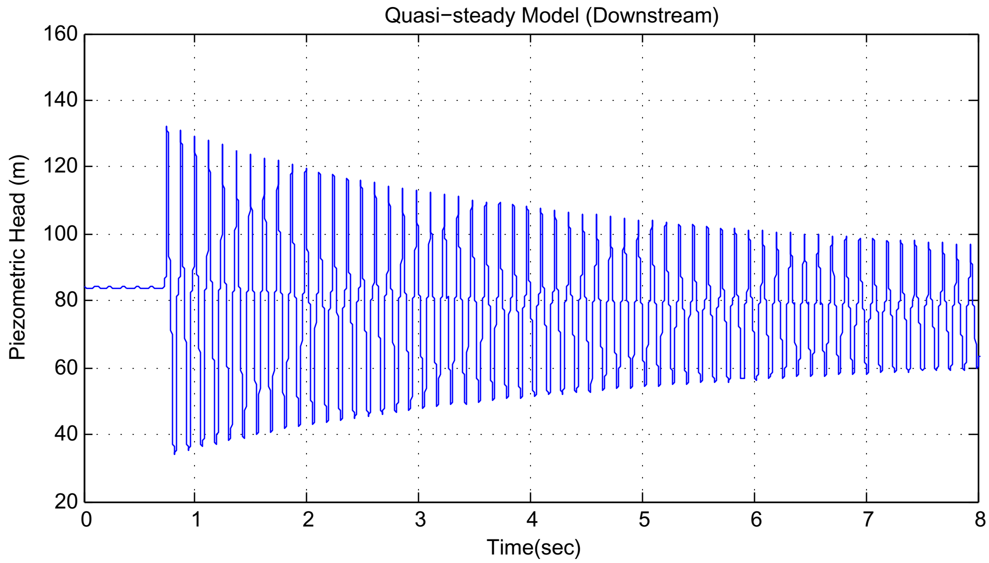

Figure 5.5: Quasi-steady Model with f = 0.15 for $0 \leq t \leq 8$

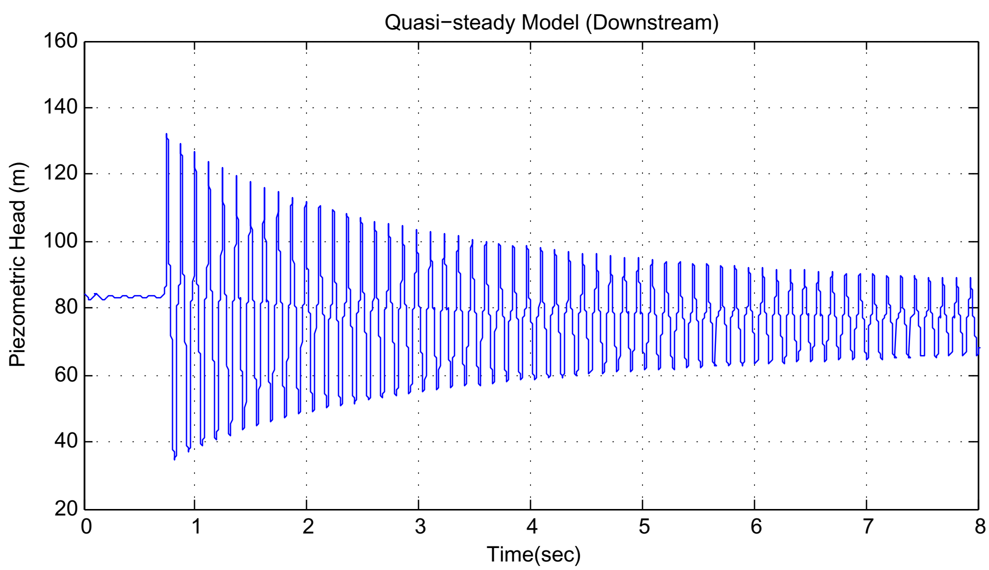

Figure 5.6: Quasi-steady Model with f = 0.3 for $0 \leq t \leq 8$

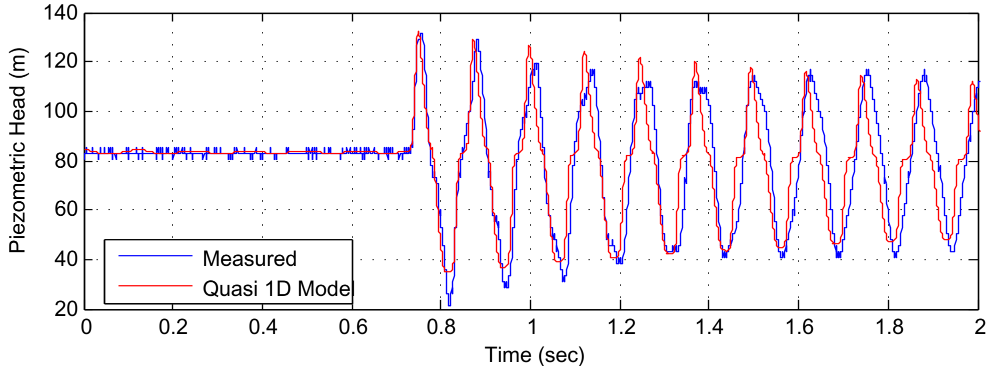

(a) $0 \le t \le 2$

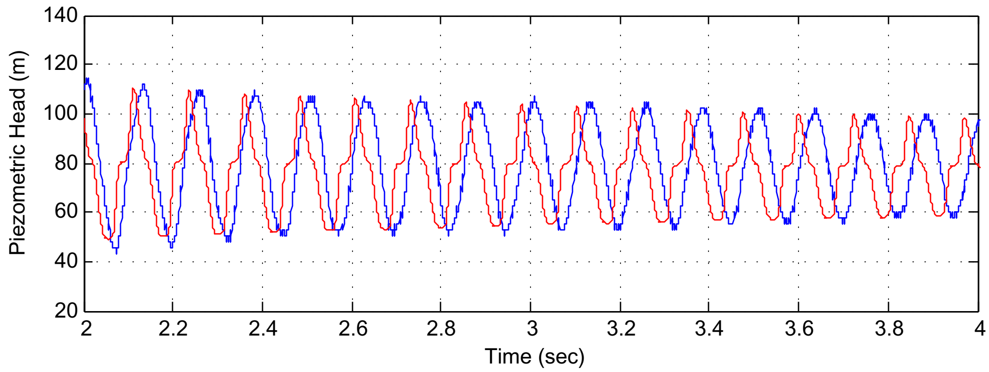

(b) $2 \le t \le 4$

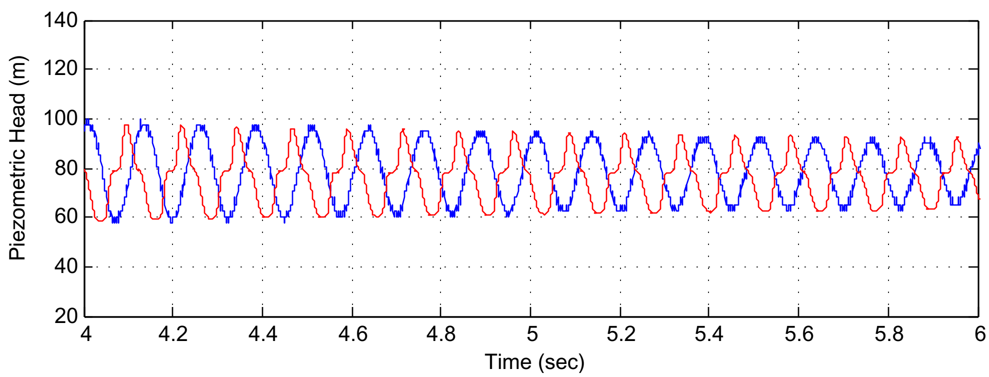

(c) $4 \le t \le 6$

Figure 5.7: Case 1 Simulated By Quasi-Steady 1D Model With $F_T = 0.3$

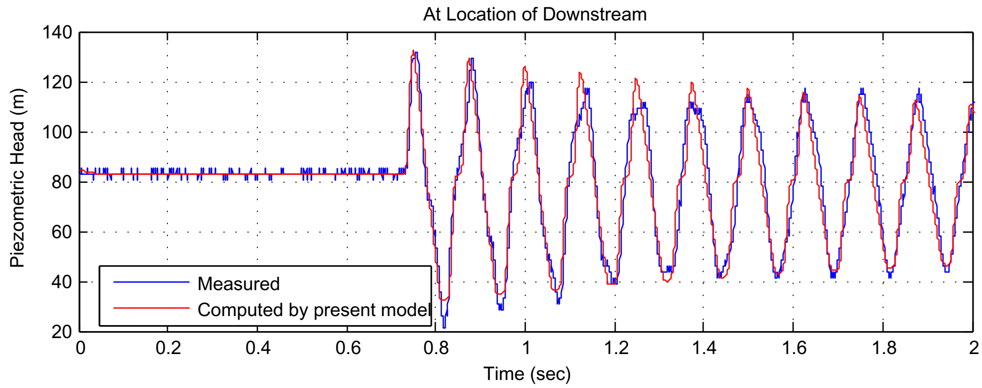

(a) $0 \leq t \leq 2$

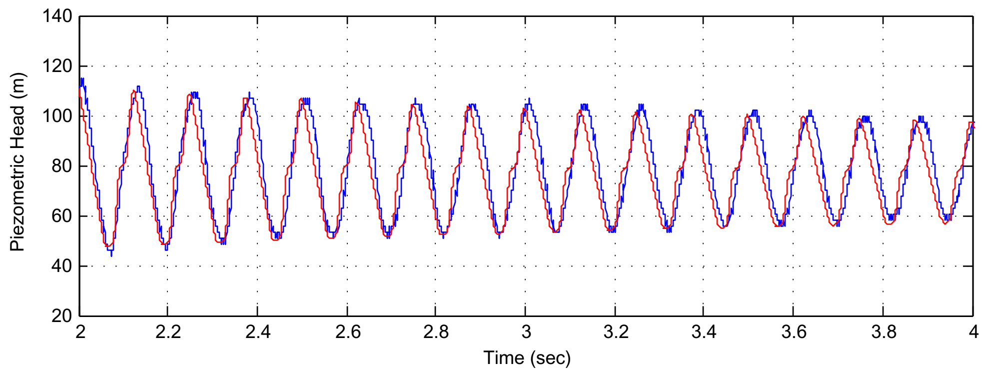

(b) $2 \leq t \leq 4$

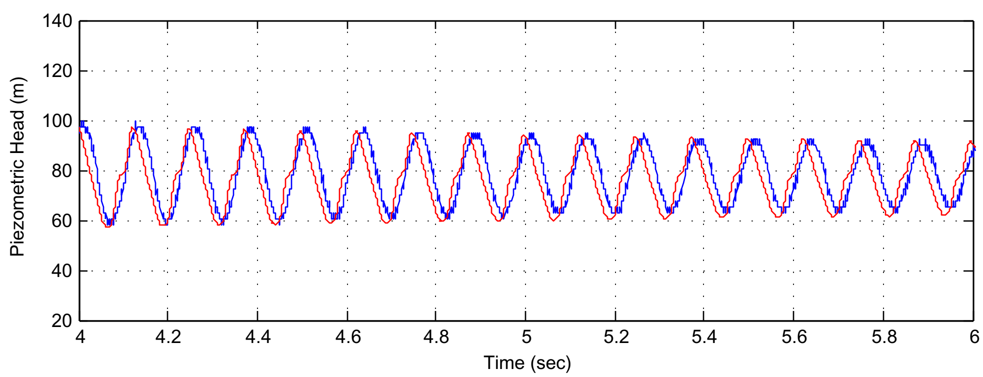

(c) $4 \leq t \leq 6$

Figure 5.8: Case 1 Simulated By Unsteady Friction 1D Model With $F_T = 0.3$ and $k_2 = 0.045$

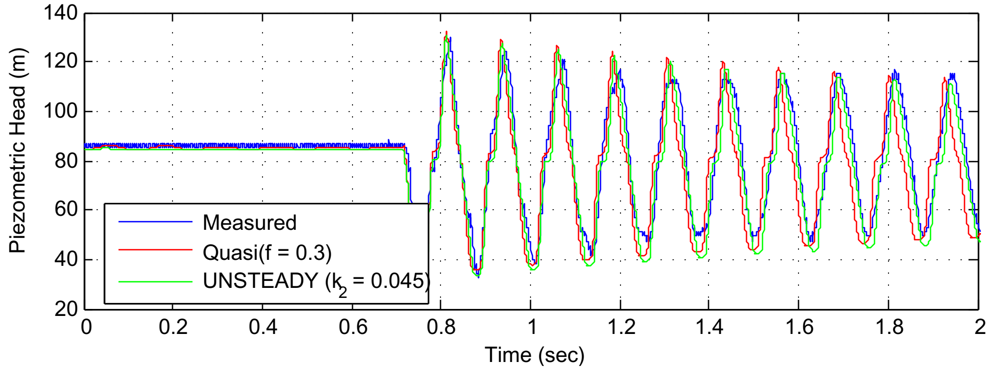

(a) $0 \leq t \leq 2$

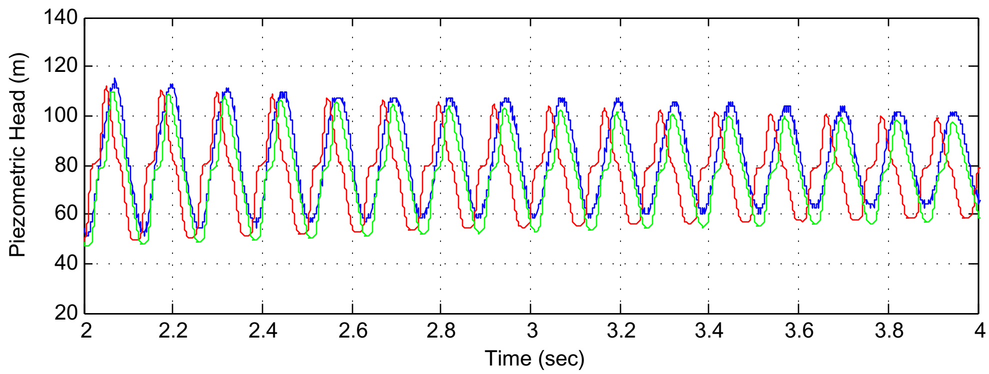

(b) $2 \leq t \leq 4$

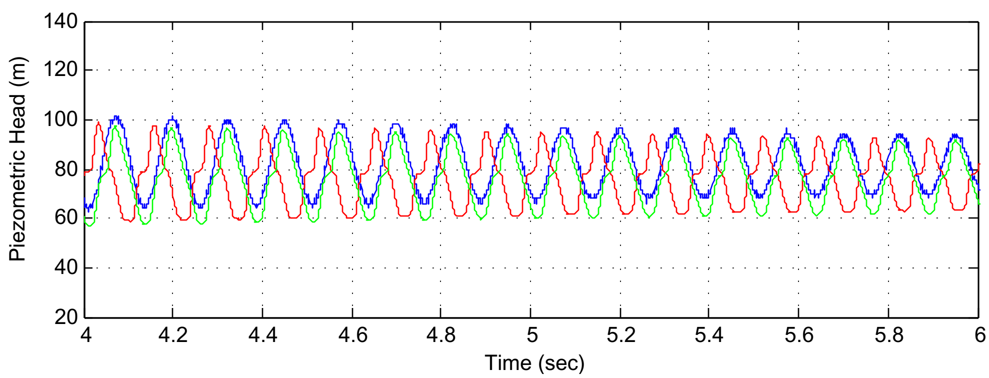

(c) $4 \leq t \leq 6$

Figure 5.9: Case 1 Comparison of Two Different Models At Upstream

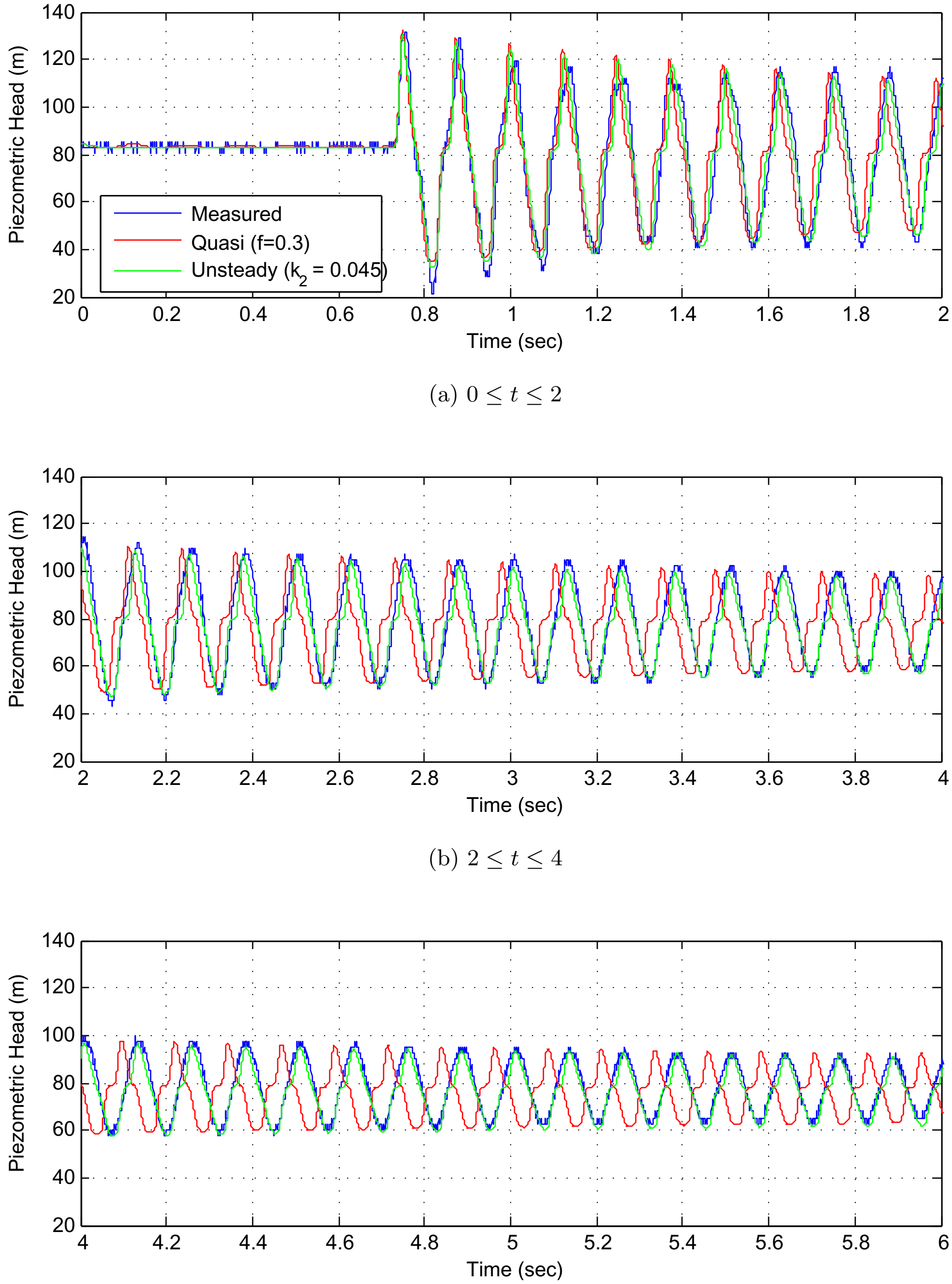

(a) $0 \leq t \leq 2$

(b) $2 \leq t \leq 4$

(c) $4 \leq t \leq 6$

Figure 5.10: Case 1 Comparison of Two Different Models At Downstream

It is noted from Fig 5.7 and 5.8 that if one is only interested in the maximum response and its decay ratio, there is no significant difference between two simulation results. However, if the phase shift of pressure wave for a long-term period of time needs to be simulated, it seems that the frequency-dependent analysis by the unsteady friction model fits better with the experiment data. Since the understanding the flow and structure interactions during the transient requires more precise model, the unsteady friction model is incorporated with a coupling model for the simulation of Case 2 where the backflow prevention assembly is set up.

The main point of the comparison here is to compare the difference between results from the traditional analysis with quasi-steady assumption and results from the frequency-dependent analysis with consideration of the additional energy loss due to unsteady friction and the phase shift of pressure waves. The numerical result for Case 1 obtained from the unsteady friction model shows a better agreement with the recorded data, hence the governing equations for the unsteady friction model are used later with the coupling model for numerical analysis of the system with a backflow prevention assembly.

5.3 Implementation of A Coupling Model: Case 2

The present model is based on the unsteady friction 1D model coupling with the motion equation of a backflow prevention assembly. In Fig 5.25 and 5.26, the simulation results by the present model are compared to the experimental record for Case 2. In the beginning modeling a backflow prevention assembly, the assembly is considered as an assembly having an internal single check valve. The total head loss coefficient (or equivalent head loss coefficient), F_T, is 0.3 inclusive of minor losses and the constant value of k_2 equals to 0.045 as same as the values for Case 1. The time histories of pressure head for the present model are shown in Figs 5.11, 5.12, 5.13, and 5.14. The changes in flow rate is shown in Fig 5.15 and the angular position of check disk which is a function of flow rate and flow acceleration is presented in Fig 5.16. In Fig 5.15, a reversal flow at maximum flow rate of $-3.514 \times 10^{-4}\, m^3/sec$ through the assembly is observed between 0.754 and 0.780 second. Most of backflow prevention assemblies are designed as an fast responding type to minimize allowable reversal flows so as to considerably enhance the effectiveness as a protective device.

5.3.1 Sensitivity of k_2

In order to look a degree of sensitivity of the parameter, k_2, the present model is then tested with different k_2 values. The computation results are shown in Figs 5.11, 5.12, 5.17, 5.18, 5.21, 5.22, 5.25, and 5.26.

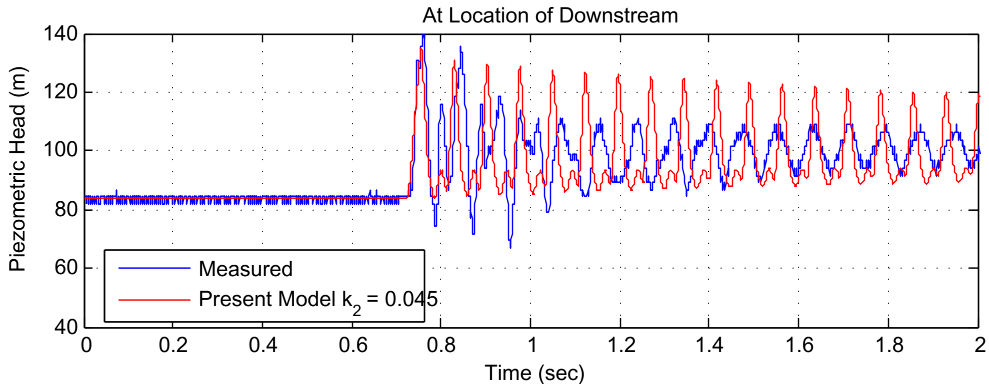

(a) $0 \leq t \leq 2$

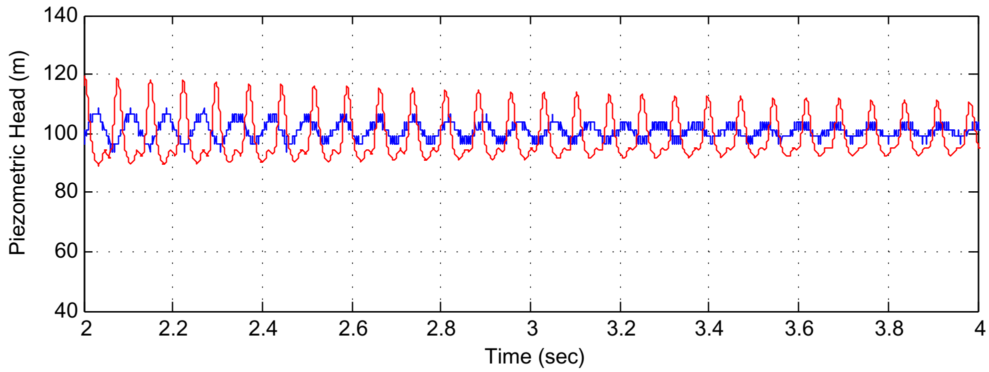

(b) $2 \leq t \leq 4$

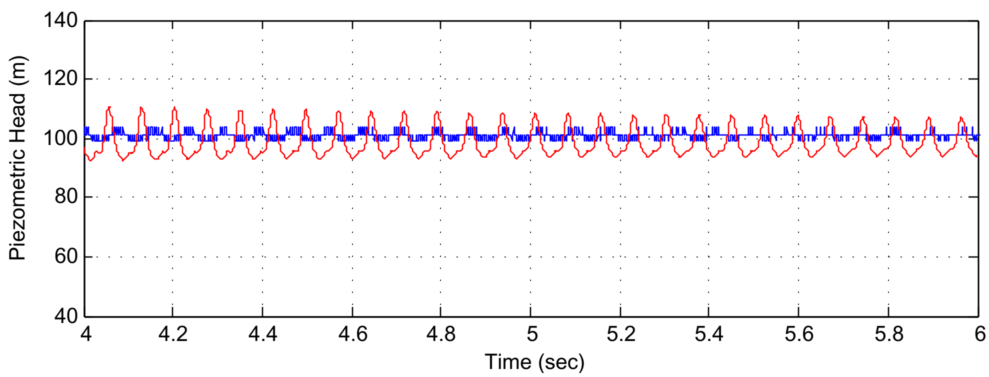

(c) $4 \leq t \leq 6$

Figure 5.11: Case 2 (Downstream) Present Model With $F_T = 0.3$ and $k_2 = 0.045$

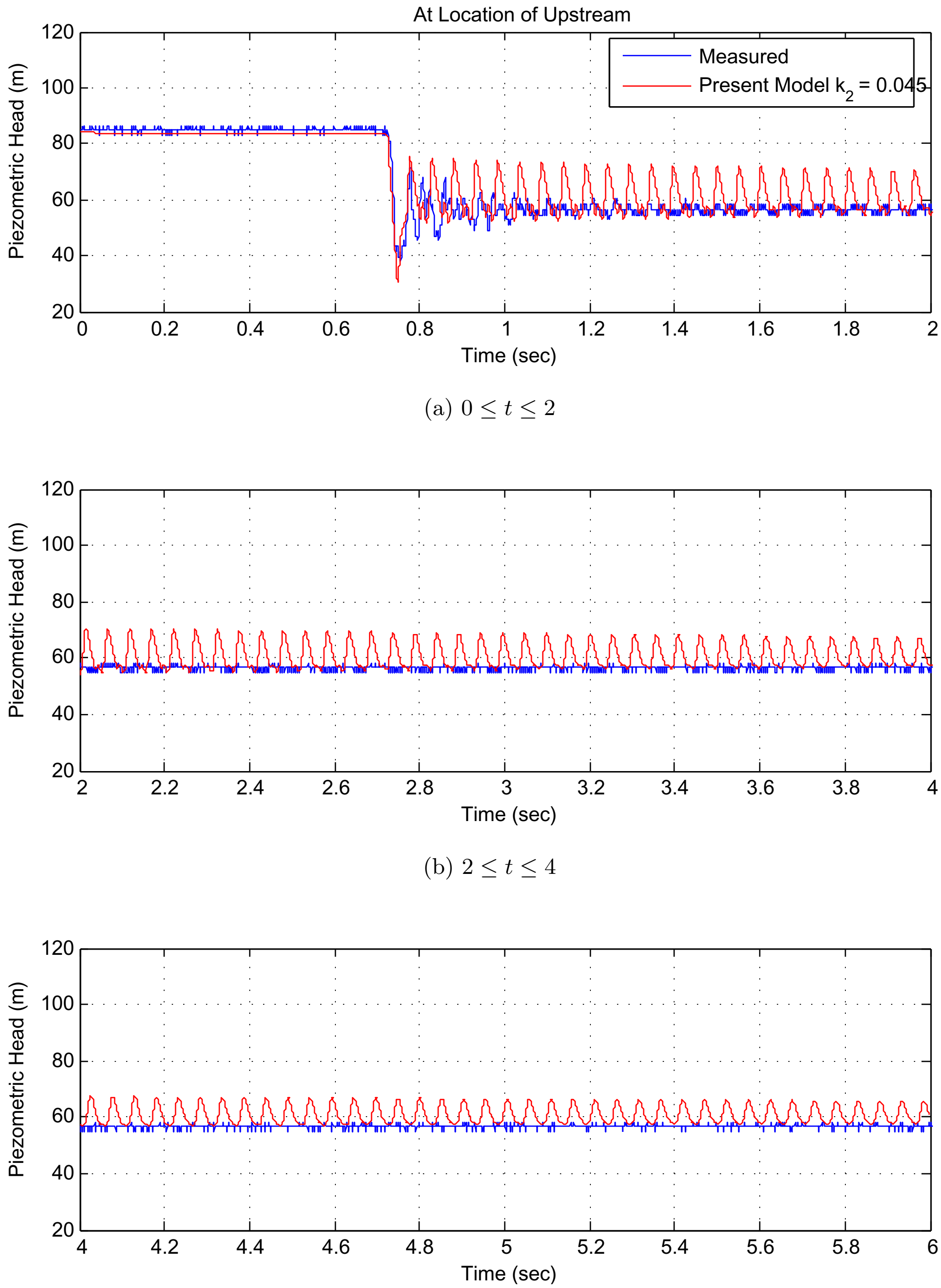

(a) $0 \leq t \leq 2$

(b) $2 \leq t \leq 4$

(c) $4 \leq t \leq 6$

Figure 5.12: Case 2 (Upstream) Present Model With $F_T = 0.3$ and $k_2 = 0.045$

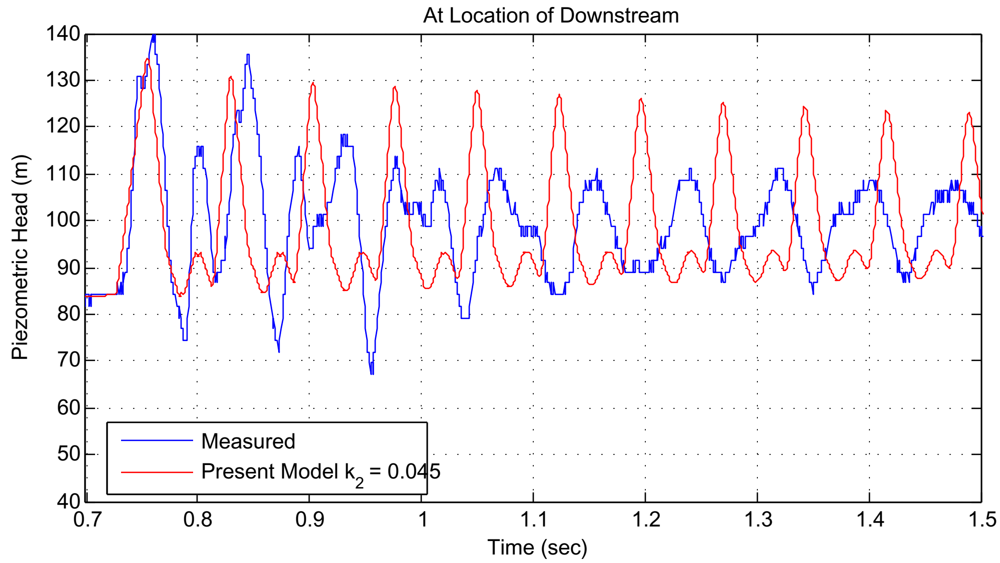

Figure 5.13: Case 2 (Downstream) Present Model $F_T = 0.3$ and $k_2 = 0.045$ for $0.7 \leq t \leq 1.5$

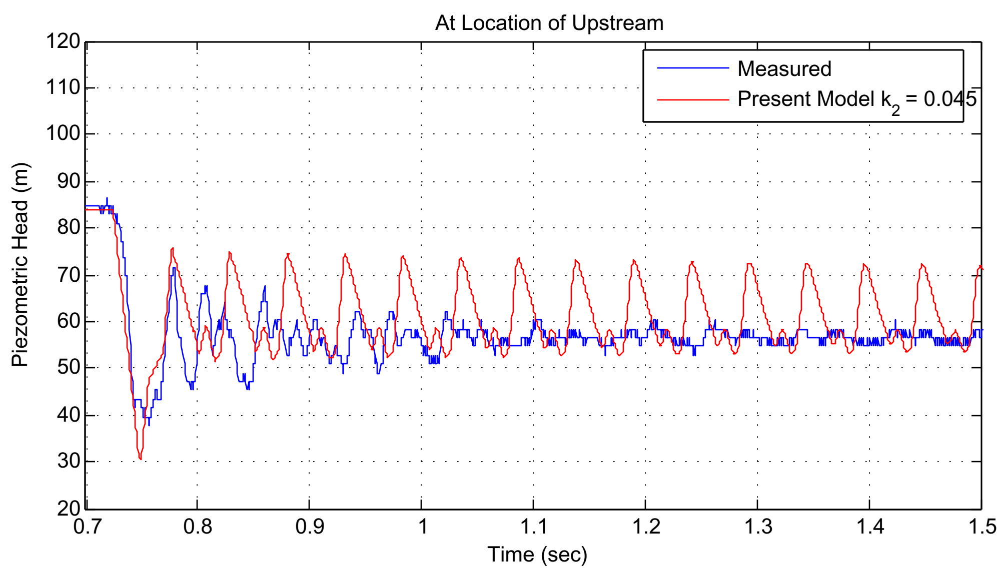

Figure 5.14: Case 2 (Upstream) Present Model $F_T = 0.3$ and $k_2 = 0.045$ for $0.7 \leq t \leq 1.5$

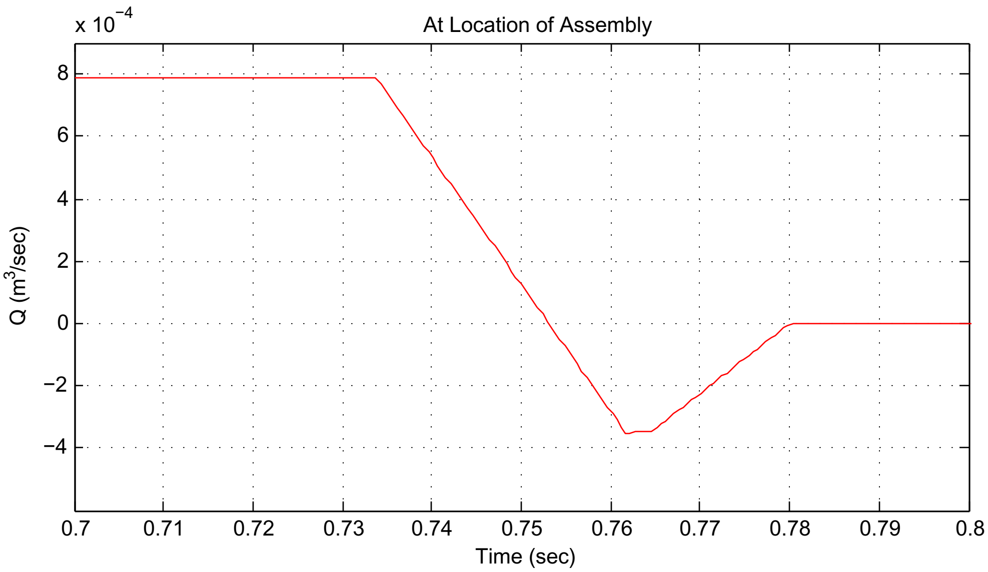

Figure 5.15: Case 2 Flow Rate Changes At Assembly for $0.7 \leq t \leq 0.8$

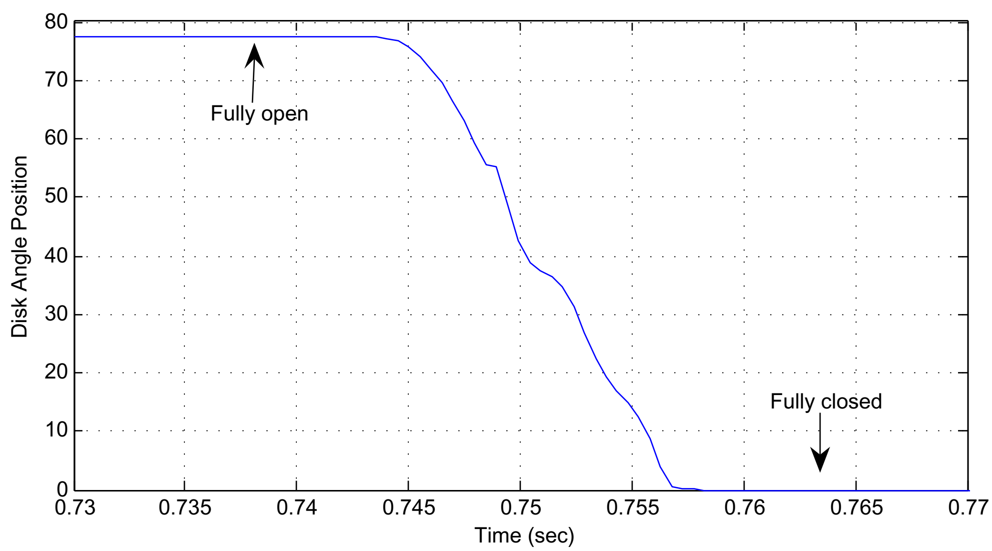

Figure 5.16: Case 2 Disk Angle Position

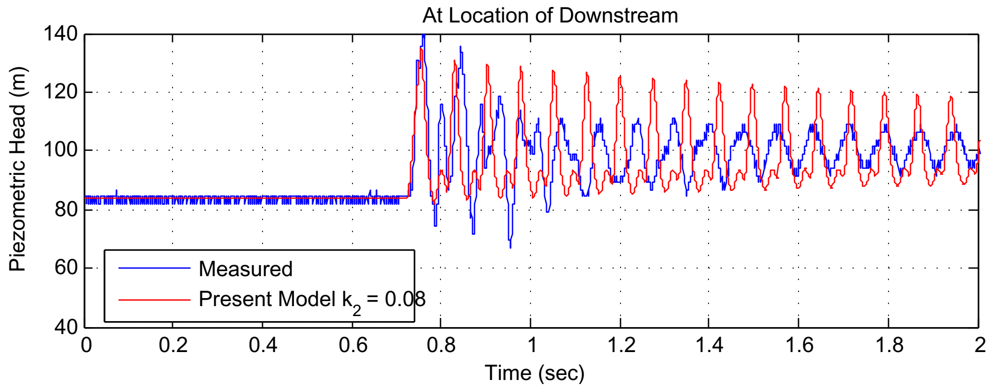

(a) $0 \leq t \leq 2$

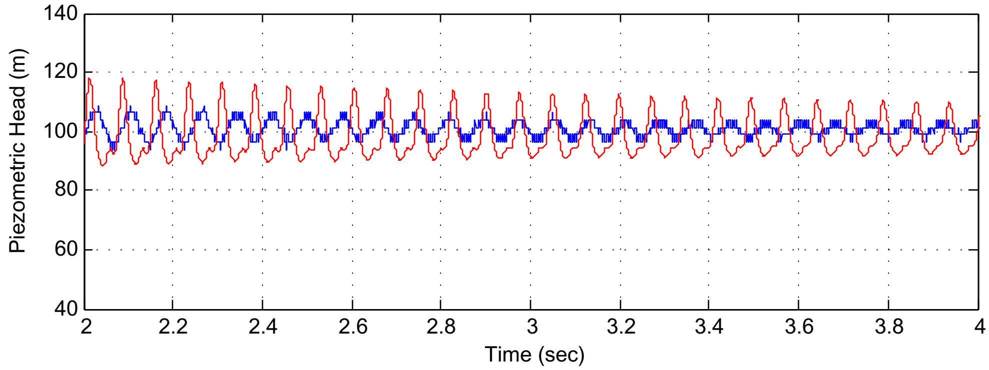

(b) $2 \leq t \leq 4$

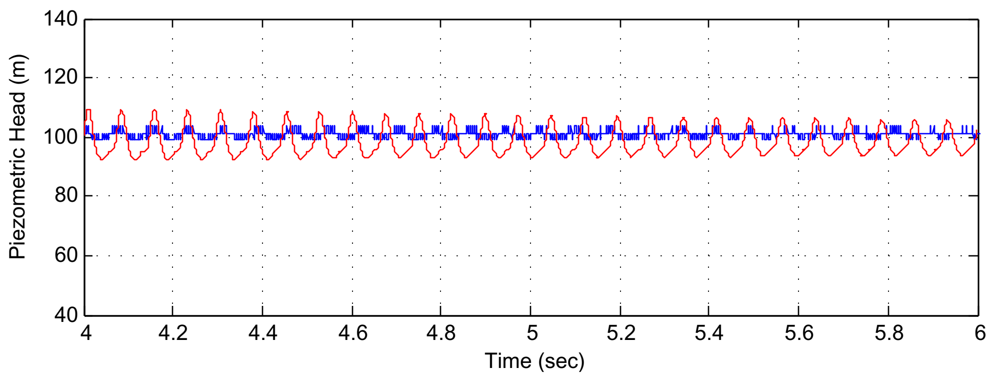

(c) $4 \leq t \leq 6$

Figure 5.17: Case 2 (Downstream) Present Model With $F_T = 0.3$ and $k_2 = 0.08$

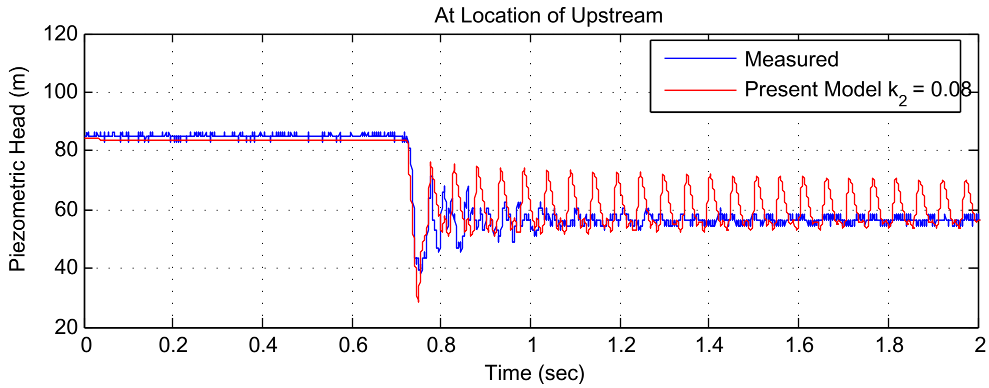

(a) $0 \leq t \leq 2$

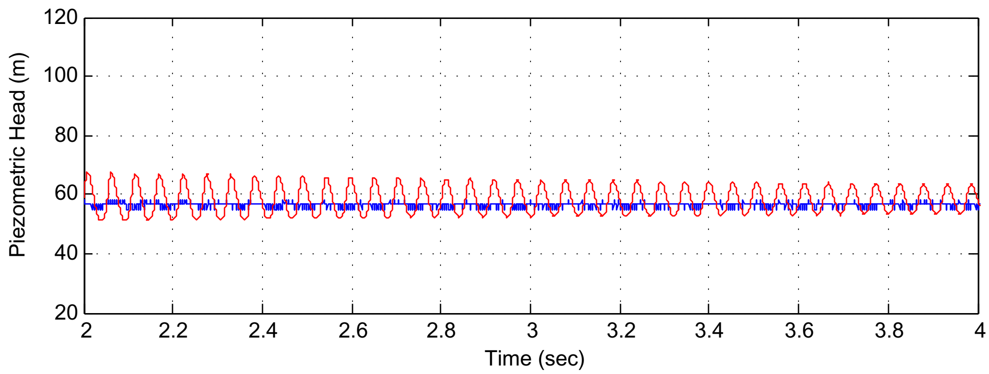

(b) $2 \leq t \leq 4$

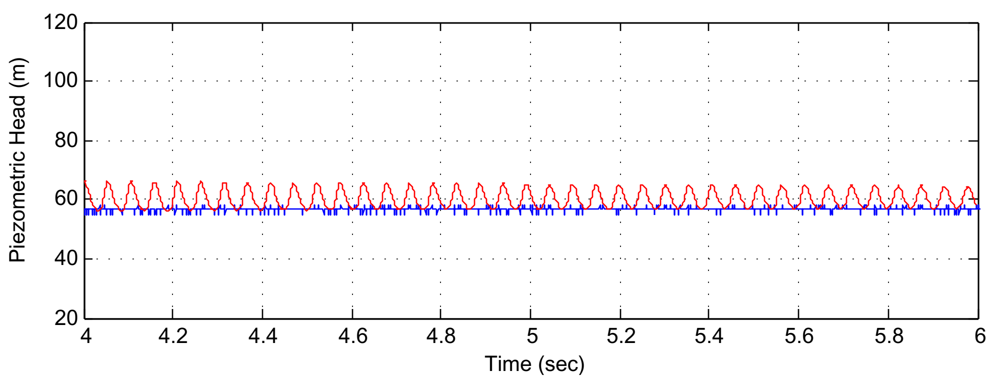

(c) $4 \leq t \leq 6$

Figure 5.18: Case 2 (Upstream) Present Model With $F_T = 0.3$ and $k_2 = 0.08$

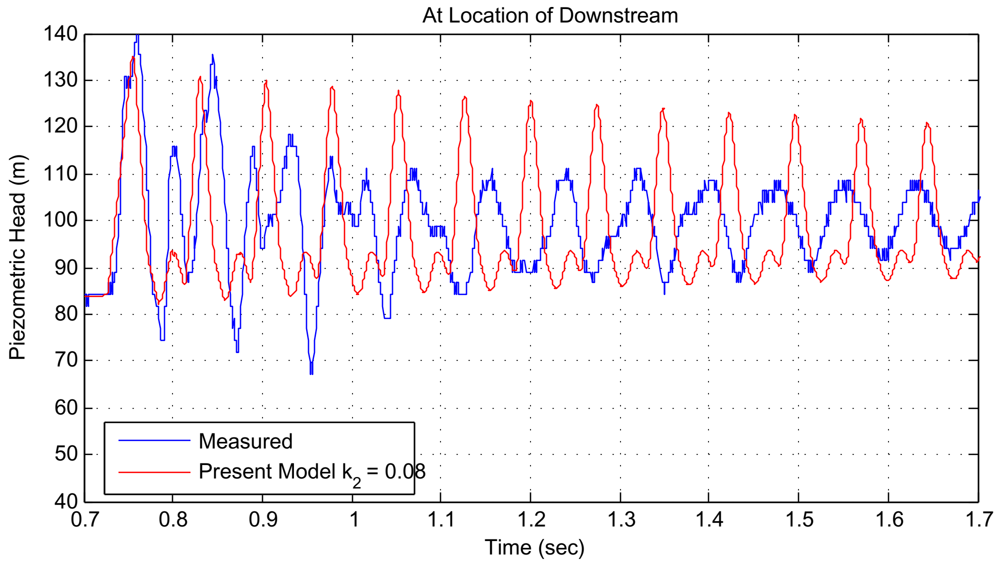

Figure 5.19: Case 2 (Downstream) Present Model $F_T = 0.3$ and $k_2 = 0.08$ for $0.7 \leq t \leq 1.5$

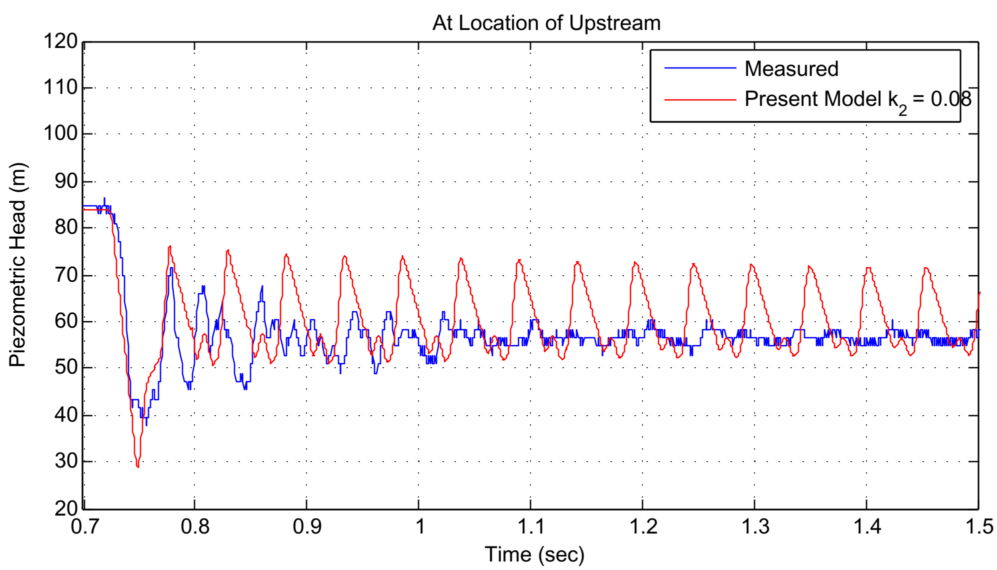

Figure 5.20: Case 2 (Upstream) Present Model $F_T = 0.3$ and $k_2 = 0.08$ for $0.7 \leq t \leq 1.5$

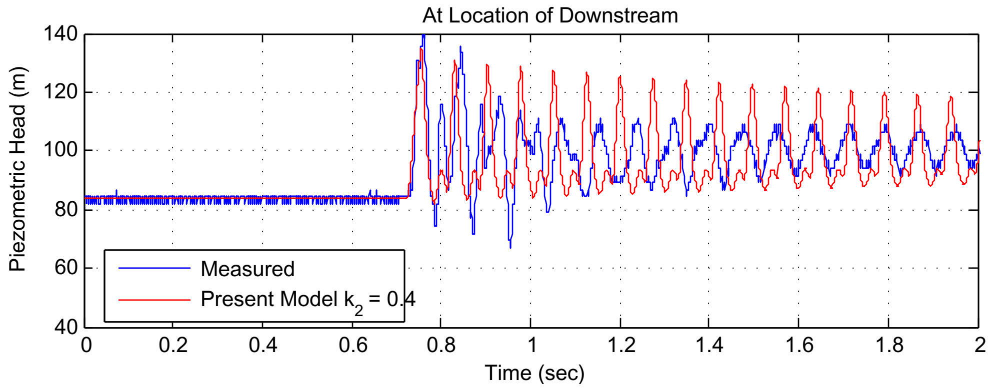

(a) $0 \leq t \leq 2$

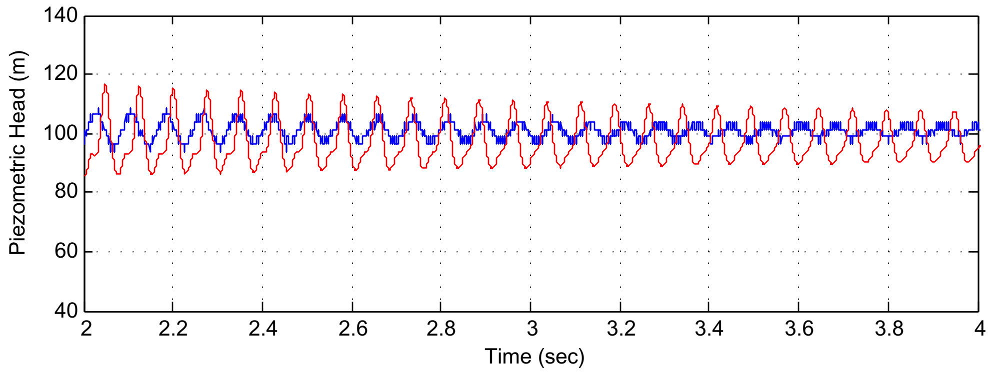

(b) $2 \leq t \leq 4$

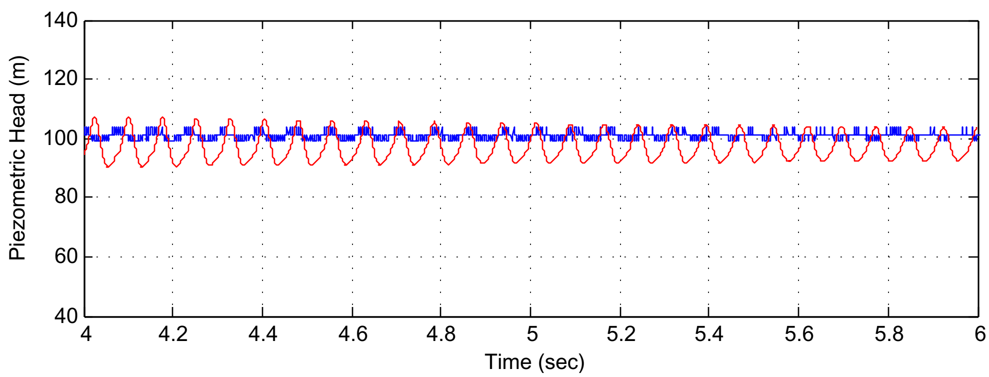

(c) $4 \leq t \leq 6$

Figure 5.21: Case 2 (Downstream) Present Model With $F_T = 0.3$ and $k_2 = 0.2$

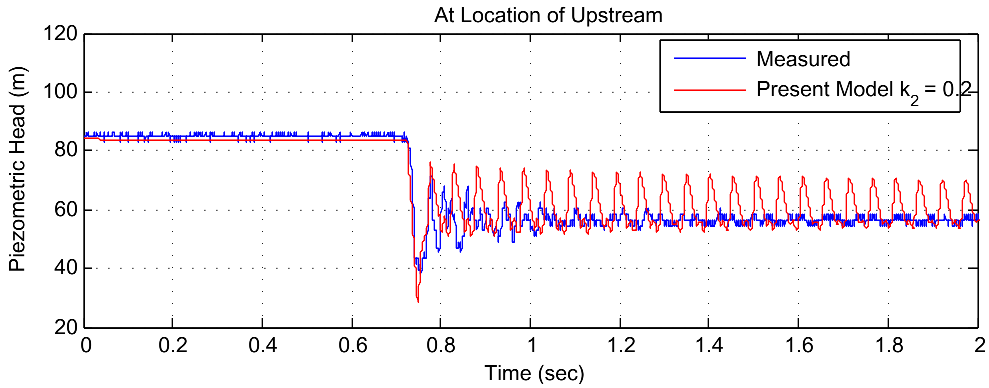

(a) $0 \leq t \leq 2$

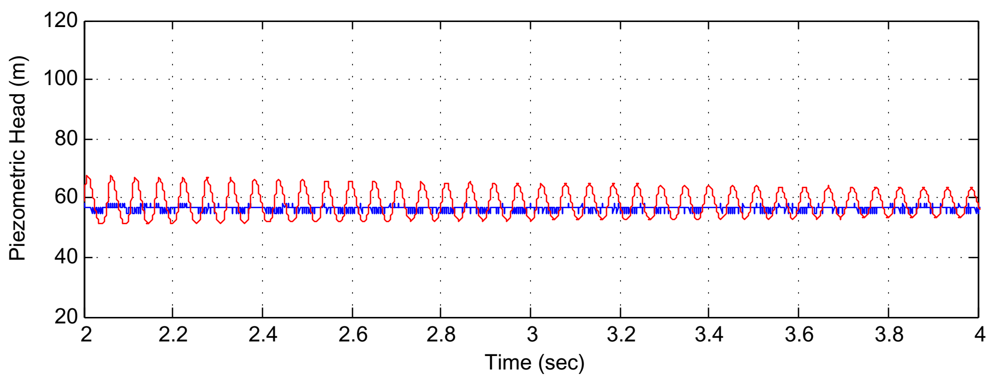

(b) $2 \leq t \leq 4$

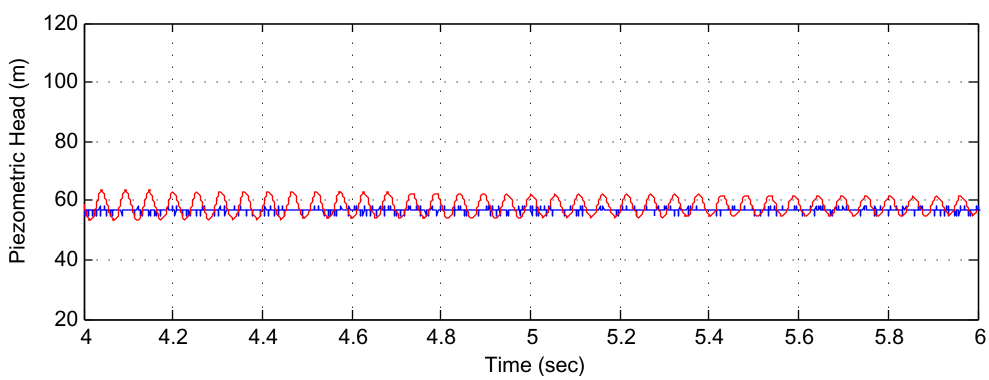

(c) $4 \leq t \leq 6$

Figure 5.22: Case 2 (Upstream) Present Model With $F_T = 0.3$ and $k_2 = 0.2$

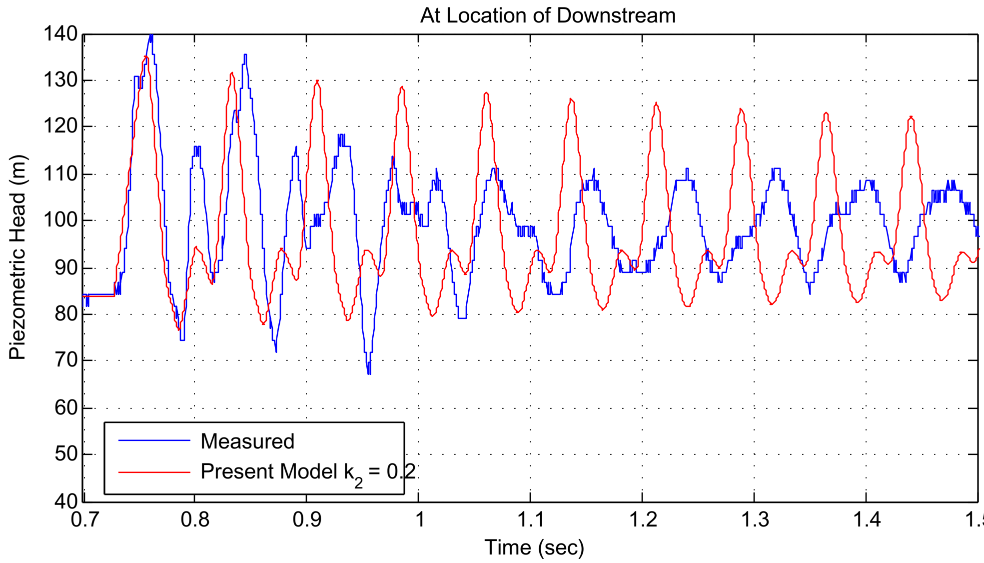

Figure 5.23: Case 2 (Downstream) Present Model $F_T = 0.3$ and $k_2 = 0.2$ for $0.7 \leq t \leq 1.5$

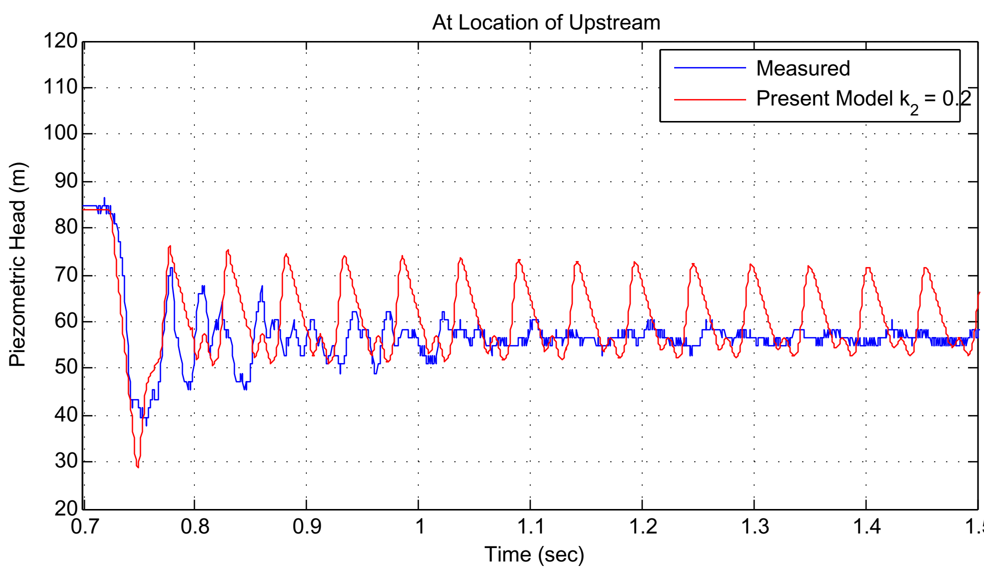

Figure 5.24: Case 2 (Upstream) Present Model $F_T = 0.3$ and $k_2 = 0.2$ for $0.7 \leq t \leq 1.5$

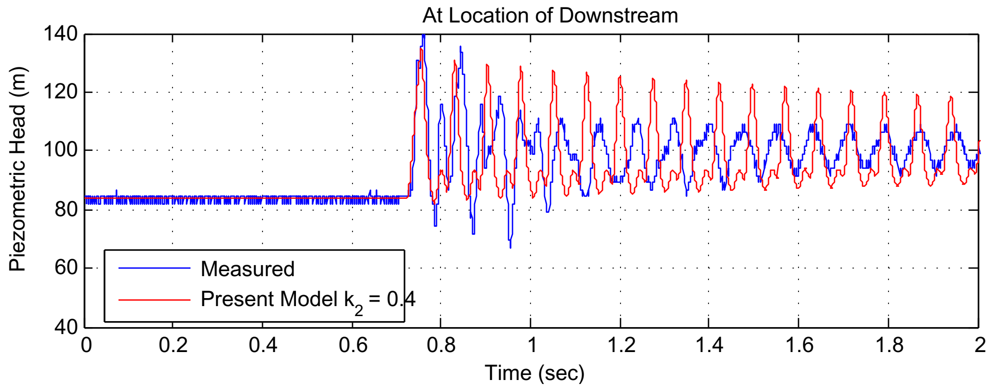

(a) $0 \leq t \leq 2$

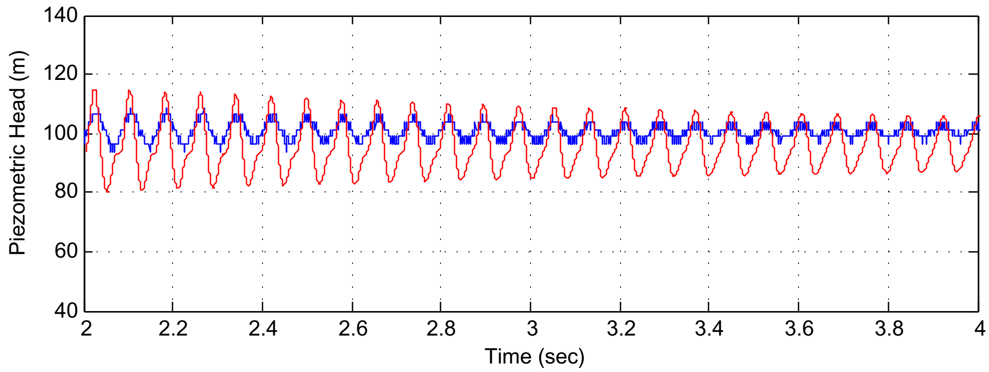

(b) $2 \leq t \leq 4$

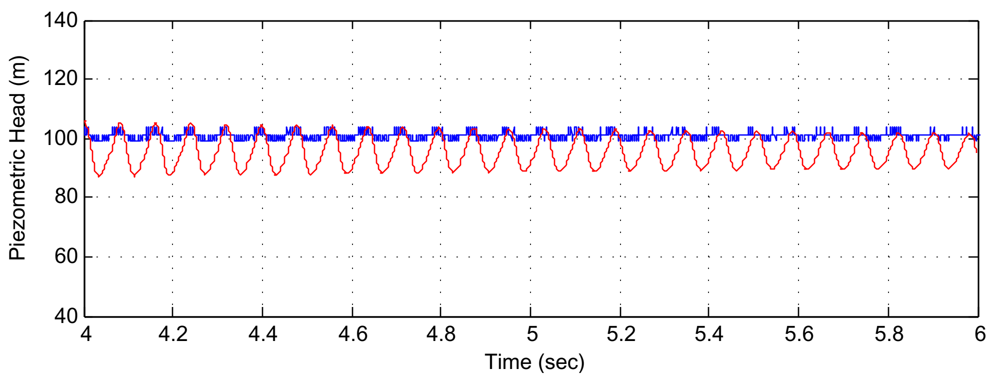

(c) $4 \leq t \leq 6$

Figure 5.25: Case 2 (Downstream) Present Model With $F_T = 0.3$ and $k_2 = 0.4$

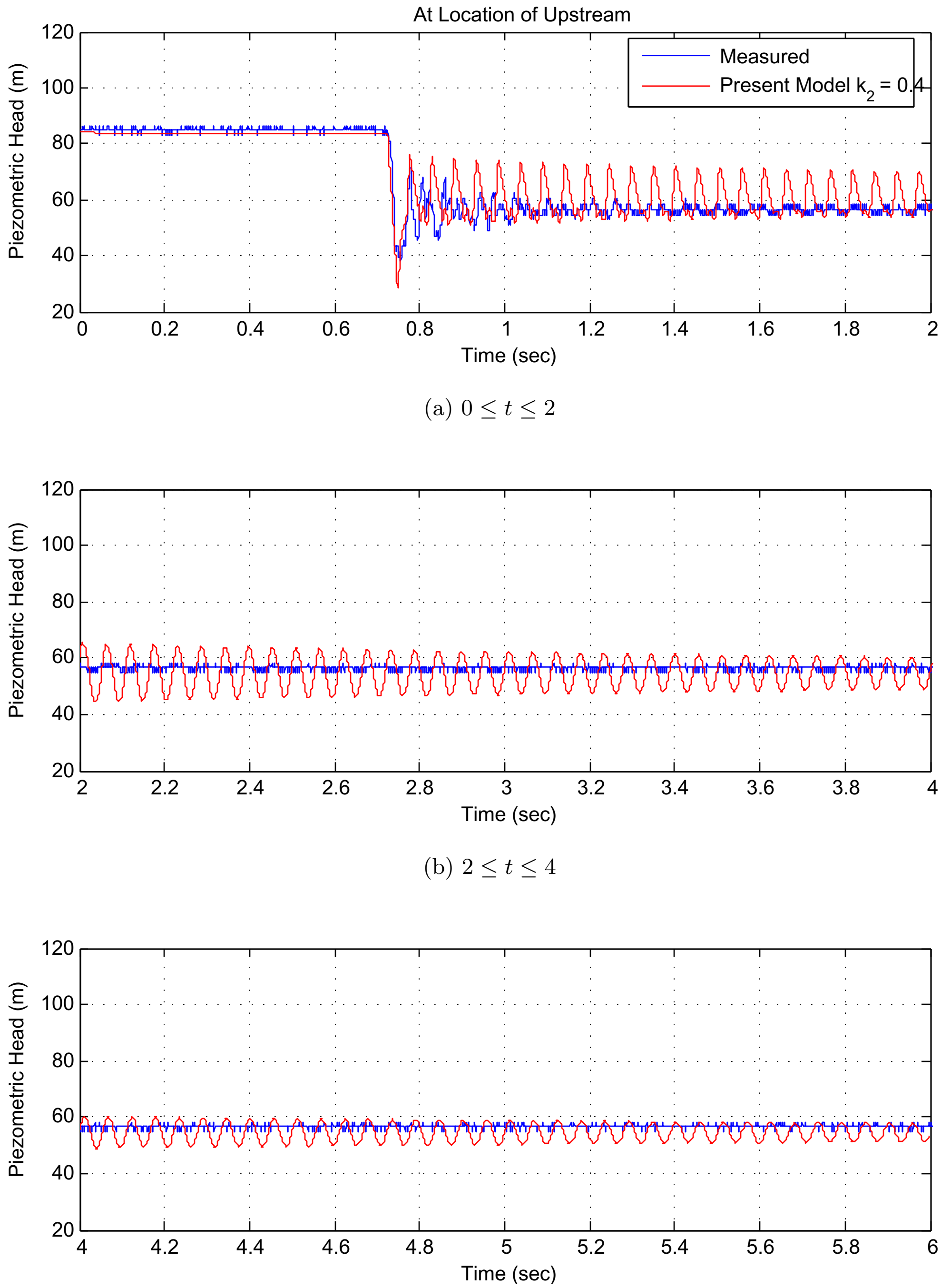

(a) $0 \leq t \leq 2$

(b) $2 \leq t \leq 4$

(c) $4 \leq t \leq 6$

Figure 5.26: Case 2 (Upstream) Present Model With $F_T = 0.3$ and $k_2 = 0.4$

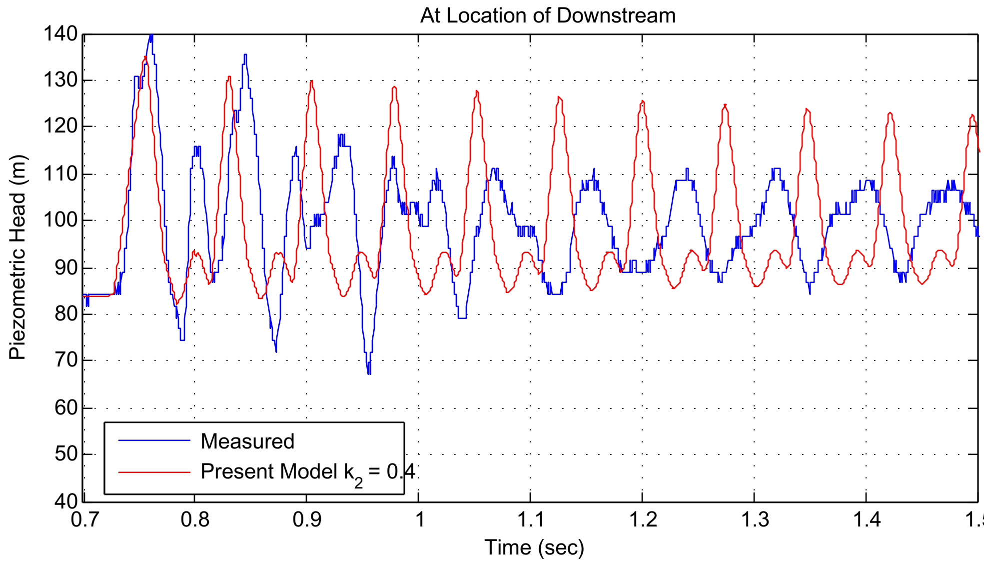

Figure 5.27: Case 2 (Downstream) Present Model $F_T = 0.3$ and $k_2 = 0.4$ for $0.7 \leq t \leq 1.5$

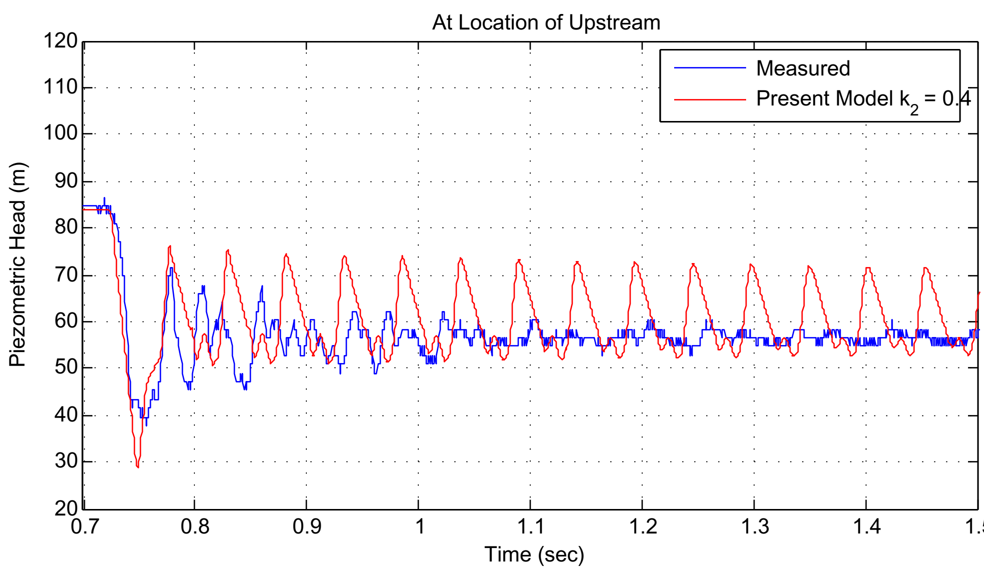

Figure 5.28: Case 2 (Upstream) Present Model $F_T = 0.3$ and $k_2 = 0.4$ for $0.7 \leq t \leq 1.5$

The discrepancies between the measured and computed results in Case 2 may be caused by the dramatic changes in the wave speed. The repetitive opening and closing movement of the check disk installed in the intermediate section of the pipe may cause the formation of vapour cavitation and the turbulent flows around the disk. As a result, the wave speed reduces causing observable phase shifts at the upstream and downstream regions. As previously observed in Figs 4.16 and 4.18, the wave speeds for Case 1 and Case 2 are different. In Fig 4.16, there found a significant energy damping at upstream after 1 second. The fluctuation at the downstream continues even after 6 seconds while the fluctuation at the upstream ends very quickly.

With the given assumption that the wave speed is held constant during oscillation, a phase shift may also occur when the flow is interfered in its direction (due to the excessive bends in the experimental set-ups).

Although different in detail, the simulated result follows general trends of valve slam phenomena. The pressure waves generated in the pipe system seems to experience a phase-shift when it encounters sudden changes in flow pattern, such as reflection, transmission, or turning direction. The phase shift seen in Fig 5.25 is much larger than that for Case 1. Also, it is clear that the energy losses across the assembly become larger than what these are expected. It is concluded that the delay of oscillation of the pressure waves and the fast energy damping effect are caused largely by the formation of cavitation and the occurrence of flow separations around the assembly.

5.3.2 Classification of Assemblies: Ideal, Undamped, And Damped

The present model is also implemented for the assemblies with three different types of the assembly (ideal, undamped and damped). The shapes, decay rates, and periods of the pressure waves created in the system are seriously affected by the assembly's behavior. Depending on the time of valve closure, the path of moving disks, and the maximum reverse flow allowance, results may be widely different. For example, in Fig 5.30, the pressure rise caused by the check valve slam is the greatest for the undamped valve. As the time of closure increases, the intensity of the pressure wave weakens.

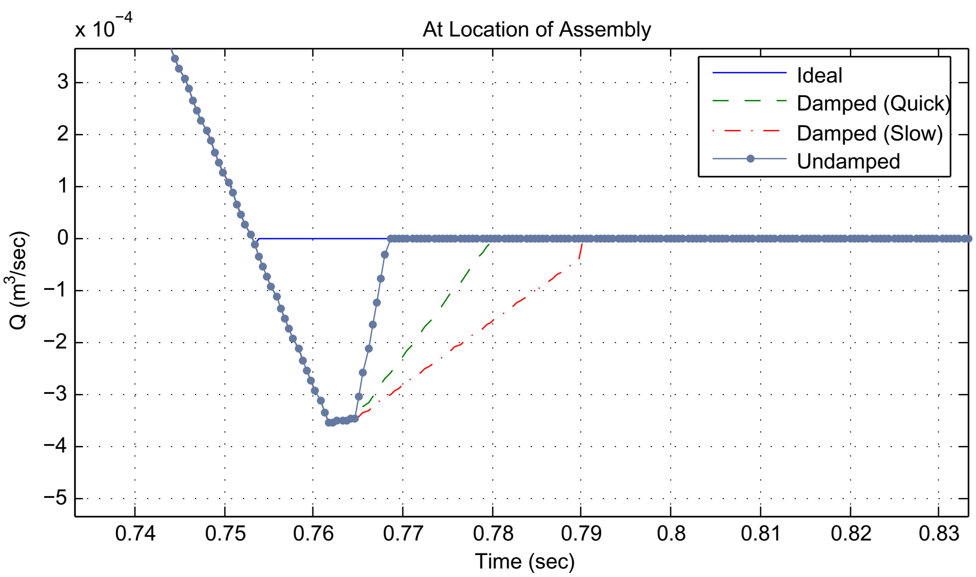

Figure 5.29: Changes on Flow Rate At Assembly

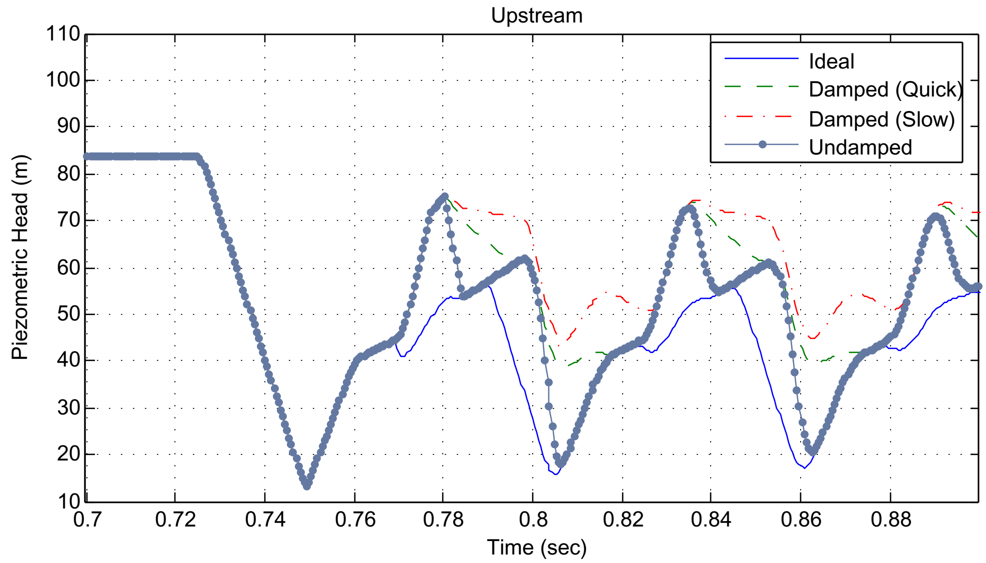

Figure 5.31: (Upstream) Comparison of Responses With Different Valve Types

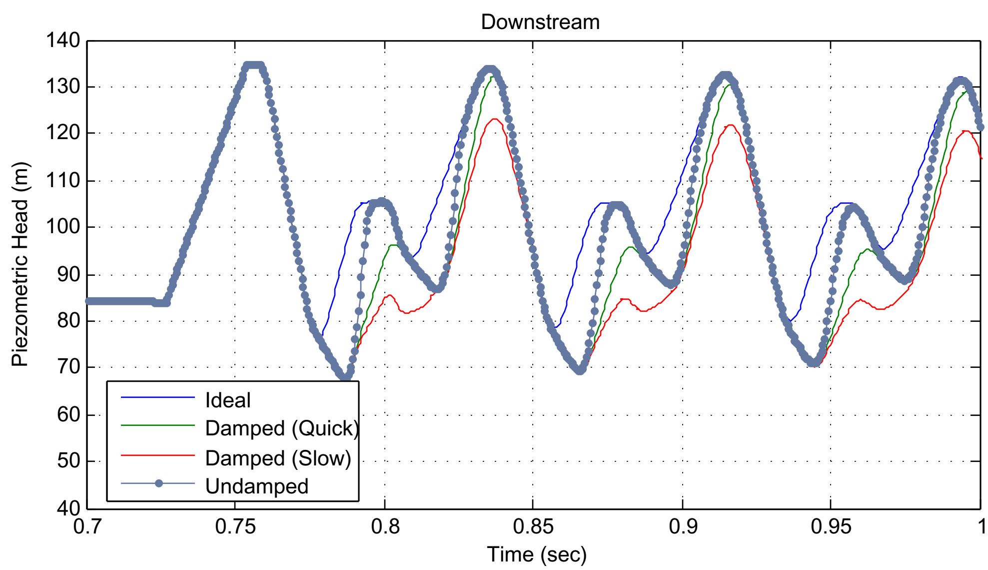

Figure 5.30: (Downstream) Comparison of Responses With Different Valve Types

Chapter 6

Conclusion And Recommendation

6.1 Summary and Conclusion

The present study contains experimental and numerical analysis for rapid transients in water distribution systems involving backflow prevention assemblies. Two sets of fundamental equations for unsteady pipe flows are examined and its numerical results solved by the method of characteristics are compared with a set of experimental data. Also, the moment-of-momentum equation developed for a backflow prevention assembly with an internal check valve has been incorporated into a coupling model for the simulation of the valve-fluid interaction, on basis of the unsteady friction 1D model. The hydraulic torque in the moment-of-momentum equation is estimated by using a valve equation relating flow to pressure drop across the assembly with the flow rate. Fourth-order Runge-Kutta integration scheme is used to solve the moment-of-momentum equation for angle increments for each time step. Pure water hammer waves are observed in Case 1 and check valve slam phenomena is observed in Case 2. Case 2 is simulated by the present model. The assembly internal valve used in the computer simulations is modeled as an ideal, undamped, damped fast-responding, and damped slow-responding type. Ideal backflow prevention assemblies close in the instant of the flow is zero, preventing backflow. In reality, however, a backflow prevention assembly allows a certain level of backflow through it. The sudden stoppage of reverse flows creates another pressure rises called check valve slam, propagating in the system.

The key equations used for the coupling model in the present study is summarized as follows:

1. Quasi-steady friction model

$$\frac{\partial H}{\partial t} + \frac{a^2}{g}\frac{\partial V}{\partial x} = 0$$
$$g\frac{\partial H}{\partial x} + \frac{\partial V}{\partial t} + \frac{f}{D}\frac{V\left|V\right|}{2g} = 0$$

2. Unsteady friction model

$$\frac{\partial H}{\partial t} + \frac{a^2}{g}\frac{\partial V}{\partial x} = 0$$
$$g\frac{\partial H}{\partial x} + \frac{\partial V}{\partial t} + \frac{f}{D}\frac{V\left|V\right|}{2} + K_2\left(\frac{\partial V}{\partial t} - a\frac{\partial V}{\partial x}\right) = 0$$

3. Wave Speed

$$a = \sqrt{\frac{K_w/\rho_w}{1 + (1 - p^2) * (K_w/E_p) * (D/e)}}$$

4. Moment-of-momentum equation

$$T_w + T_e + T_f + T_h = I\frac{d^2\theta}{dt^2}$$

5. Hydraulic torque, T_h

$$
\begin{aligned}
T_h &= \gamma \Delta H \bar{r} A_v \\
&= \frac{\gamma \bar{r} A_v Q \left| Q \right|}{2g(C_d A_o)^2}
\end{aligned}
$$

6. Valve discharge, Q_v

Positive flow:

$$
\begin{aligned}
Q_v &= -C_v \left(B_{P1} + B_{M2}\right) + \sqrt{C_v^2 \left(B_{P1} + B_{M2}\right)^2 + 2C_v \left(C_{P1} - C_{M2}\right)} \\
& \quad when \ C_{P1} - C_{M2} \geq 0
\end{aligned}
$$

Negative flow:

$$
\begin{aligned}
Q_v &= C_v \left(B_{P1} + B_{M2}\right) - \sqrt{C_v^2 \left(B_{P1} + B_{M2}\right)^2 - 2C_v \left(C_{P1} - C_{M2}\right)} \\
& \quad when \ C_{P1} - C_{M2} \leq 0 \\
& \quad or \\
&= 0 \\
& \quad for \ \ ideal \ \ valve
\end{aligned}
$$

The conclusions made from this present study are as follows:

1. The sudden changes in flow rate at both ends of pipeline create excessive pressure rises in the distribution system.

2. The pressure waves created in the distribution system propagate at the speed of wave and decay with time.

3. The speed of pressure waves is assumed to be a constant for the present models. However, the measurement shows a significant reduction in the wave speed and an observable phase shift.

4. The damping of the pressure fluctuations in the system under transient conditions is considerably greater than that estimated by the steady state friction relationship.

5. The quasi-steady approximation clearly exhibits the discrepancies between the experimental data and computer calculation, in magnitude and phase of pressure waves particularly for long-time-period records of rapid transient events.

6. The present model with the equivalent loss coefficient, F_T, using the method of characteristics is successfully implemented to simulate additional energy losses due to the unsteady friction effect during water hammer events.

7. To simulate the dynamic behavior of a backflow prevention assembly when pressure waves pass through the assembly, the water hammer equations (continuity and momentum equations) are solved for each time step simultaneously with the moment-of-momentum equation of a swinging check disk installed inside the backflow prevention assembly.

8. A review of time history curve indicates that when a rapid transient occurs, the oscillatory waves are decayed quickly and delayed due to the phase shift.

9. The significant damping and phase shift of the pressure fluctuations when a backflow prevention assembly is installed within the system, are observed in the mea-

surement. The changes in fluid properties due to air entrainment and cavity formation in the assembly may result in significant reduction in the wave speed.

10. Also, the excessive bends in the experimental set-up is a major feature that may influence on the wave speed.

11. The property of pipe wall materials and the rigidity of systems may influence the intensity of water hammer waves.

12. Cavity due to the repetitive opening and closing movement of a check valve disk, turbulent effects, uncertainties of measurement and input data, approximate description of boundary conditions, and the systematic errors in the numerical model cause the deformation of the water hammer waves.

13. Local flow separation caused by the motion mechanism of backflow prevention assemblies during the transients have the biggest influence on energy dissipation and wave speeds for the initial time of the transient event.

14. The energy losses due to a backflow prevention assembly itself (not caused by friction) in the upstream region are much greater than the energy losses in the downstream region, resulting in the different damping ratio.

15. Precise modeling of a backflow prevention assembly is essential to obtain good computer results of transient modeling.

6.2 Recommendation

This research represents a study of the numerical modeling for the unsteady pipe flow and for the dynamic behavior of a backflow prevention assembly with a single internal valve when it interacts with changes of flows in a closed conduit system. The present model is not complete but effective for the rapid transient modeling. The future study will extend to the study for the additional affecting factors on the water hammer wave formation, propagation, and energy dissipation. There are many problems involved in modeling different types of assemblies to deal with the unsteady friction term. This does seem to be a very fruitful area for further research.

Bibliography

[1] B. Brunone, U. Golia, and M. Greco. Modelling of fast transients by numerical methods. In *International meeting on hydraulic transients with water column separation, 9th Round Table, IAHR*, pages 273–282, Valencia, Spain, 1991.

[2] B. Brunone, U. Golia, and M. Greco. Some remarks on the momentum equations for fast transients. In *International meeting on hydraulic transients with water column separation, 9th Round Table, IAHR*, pages 201–209, Valencia, Spain, 1991.

[3] M. Carstens and J. Roller. Boundary-shear stress unsteady turbulent pipe flow. *Journal of the Hydraulics Division, American Society of Civil Engineers.*, 85(HY2):67–81, 1959.

[4] M. Chaudhry. *Applied Hydraulic Transients*. Van Nostrand Reinhold in New York, 2nd edition, 1987.

[5] A. K. H. Koetizer and C. Lavooij. Dynamic behavior of large non-return valves. In *Procs. 5th Int. Conf. on Pressure Surges*, Hannover, 1986.

[6] C. Jaeger. *Theorie Generale du Coup de Belier*. Dunod, Paris, 1933.

[7] C. Jaeger. *Engineering Fluid Mechanics*. Blackie, London, 1956.

[8] N. Joukowski. ber den hydraulischen stoss in wasserleitungsrhren (in german), on the hydraulic hammer in water supply pipes. *Proceedings of the Annual Convention: American Water Works Association.* Translated from German By O Simin 1904.

[9] R. O. J.W. Daily, W.L. Hankey and J. Jordan. Resistance coefficient for accelerated and decelerated flows through smooth tubes and orifices. *Trans. ASME*, 78(7):1070–1077, 1956.

[10] H. J. Kwon. *Transient Flow In Water Distribution System*. PhD thesis, University of Southern California, 2005.

[11] E. P. Management. *Control Valve Handbook*. Fisher Controls International LLC, 4th edition, 2005.

[12] J. Parmakian. *Water-Hammer Analysis*. Prentice-Hall Englewood, 1st edition, 1955.

[13] G. Provoost. The dynamic behavior of non-return valves. In *Procs. 3rd Int. Conf. on Pressure Surges*, Canterbury, 1980.

[14] G. Provoost. The dynamic characteristic of non-return valves. In *11th IAHR Symp. of the Section on Hydraulic Machinery, Equipment and Cavitation, Operation Problems of Pump Stations and Power Plants*, Amsterdam, 1982.

[15] G. Provoost. A critical analysis to determine the dynamic characteristic of non-return valves. In *Procs. 4th Int. Conf. on Pressure Surges*, Bath, 1983.

[16] G. Rich. Waterhammer analysis by the laplace-mellin transformations. *Transacitions of ASME*, pages 1944–1945, 1944.

[17] G. Rich. *Hydraulic Transients*. McGraw-Hill, New York, 1st edition, 1951.

[18] V. Streeter and C. Lai. Waterhammer analysis including fluid friction. *Transactions of American Society of Civil Engineers*, (128):1491–1524, 1963.

[19] V. Streeter and E. Wylie. *Hydraulic Transients*. McGraw-Hill, New York, 1967.

[20] A. Thorley. Dynamic response of check valves. In *Procs. 4th Int. Conf. on Pressure Surges*, Bath, 1983.

[21] A. Thorley and J. Oei. Dynamic behavior of a swing check valve. In *11th IAHR Int. Symp. on Water Column Separation*, Obernach, 1981.

[22] A. Trikha. An efficient method for simulating frequency-dependent friction in transient liquid flow. *Journal of Fluids Engineering*, 97(1):97–105, 1975.

[23] A. Vardy and J. Brown. Transient, turbulent, smooth pipe friction. *Journal of Hydraulic Research.*, 33(4):435–456, 1995.

[24] A. Vardy and J. Brown. Transient turbulent friction in smooth pipe flows. *Journal of Sound and Vibration.*, 259(5):1011–1036, 2003.

[25] A. Vardy and J. Brown. Efficient approximation of unsteady friction weighting functions. *Journal of Hydraulic Engineering.*, 130(11):1097–1107, 2004.

[26] A. Vardy and J. Brown. Transient turbulent friction in fully-rough pipe flows. *Journal of Sound and Vibration.*, 270(1-2):233–257, 2004.

[27] D. J. Wood. Waterhammer analysis-essential and easy (and efficient). *Journal of Environmental Eng.*, 131(8):1123–1131, 2005.

[28] E. Wylie and V. Streeter. *Fluid transients in systems.* Prentice-Hall, 2nd edition, 1993.

[29] W. Zielke. Frequency-dependent friction in transient pipe flow. *Journal of Basic Eng.*, 90(1):109–115, 1968.